Coupled hydro-mechanical hypoplastic model for partially saturated soils under monotonic and cyclic loading

M. Pico[1] · D. Mašín[1] · W. Fuentes[2]

Abstract

Numerous geotechnical applications are significantly influenced by changes of moisture conditions, such as energy geostructures, nuclear waste disposal storage, embankments, landslides, and pavements. Additionally, the escalating impacts of climate change have started to amplify the influence of severe seasonal variations on the performance of foundations. These scenarios induce thermo-hydro-mechanical loads in the soil that can also vary in a cyclic manner. Robust constitutive numerical models are essential to analyze such behaviors. This article proposes an extended hypoplastic constitutive model capable of predicting the behavior of partially saturated fine-grained soils under monotonic and cyclic loading. The proposed model was developed through a hierarchical procedure that integrates existing features for accounting large strain behavior, asymptotic states, and small strain stiffness effects, and considers the dependency of strain accumulation rate on the number of cycles. To achieve this, the earlier formulation by Wong and Mašín (CG 61:355–369, 2014) was enhanced with the Improvement of the intergranular strain (ISI) concept proposed by Duque et al. (AG 15:3593–3604, 2020), extended with a new modification to predict the increase in soil stiffness with suction under cyclic loading. Furthermore, the water retention curve was modified with a new formulation proposed by Svoboda et al. (AG 18:3193–3211, 2023), which reproduces the nonlinear dependency of the degree of saturation on suction. The model's capabilities were examined using experimental results on a completely decomposed tuff subjected to monotonic and cyclic loading under different saturation ranges. The comparison between experimental measurements and numerical predictions suggests that the model reasonably captures the monotonic and cyclic behavior of fine-grained soil under partially saturated conditions. Some limitations of the extended model are as well remarked.

Keywords Constitutive modeling · Cyclic loading · Hypoplasticity · Intergranular strain · Unsaturated fine-grained soils

1 Introduction

The prediction of the hydro-mechanical unsaturated soil behavior under cyclic loading is relevant for different geotechnical analyses such as energy geostructures, nuclear waste disposal storage, embankments, landslides, pavements, and the pronounced seasonal fluctuations driven by climate change. Its numerical simulation through boundary value problems (BVPs) requires robust constitutive models able to represent the main features of unsaturated soils under monotonic and cyclic loading. However, properly modelling such behavior is not a simple task, since soils under unsaturated conditions are porous materials composed by three phases: mineral grains, water and air. For that reason, the stress state description for saturated soils has to be generalized for unsaturated states considering the following three fundamental effects: (a) volume change behavior due to suction or degree of saturation changes, (b) suction effects on shear strength of the soil and (c) the hydraulic behavior associated with suction changes, which also causes coupled variations in the stress state [32, 35, 53]. More challenges arise when cyclic loading wants to be addressed under unsaturated conditions, for instance small strain stiffness is directly influenced by changes in suction/degree of saturation, as well as the strain rate of accumulation. Moreover, most of the existing

✉ M. Pico
   picoduam@natur.cuni.cz

1   Charles University, Prague, Czech Republic

2   Pontificia Universidad Javeriana, Bogota, Colombia

constitutive models [1, 7, 9, 34, 36, 39] and experimental observations [4, 5, 47, 48, 50] that accounts for cyclic behavior have been tested under undrained conditions, while there is rather few literature related to unsaturated response, which is even at constant water conditions closer to a drained response due to compressibility of pore space.

Some attempts were performed using the hypoplastic framework to propose new models to reproduce the behavior of unsaturated fine-grained soils. Mašín and Khalili [22] initially proposed a model for unsaturated fine-grained soils at medium and large strains, i.e. for monotonic loading. This model was later enhanced in Wong and Mašín [51] by considering water retention features developed by Mašín [17] and the intergranular strain (IS) concept, proposed by Niemunis and Herle [31]. The resulting model was able to reproduce small strain effects and large strain asymptotic behavior. However, recent works have demonstrated that although hypoplastic models with IS present improved predictions capabilities under cyclic loading, the rates of accumulation are not adequately reproduced since it assumes a constant strain accumulation rate with an increasing number of cycles [3, 6, 44, 45], which disagrees with the experimental variation of the accumulation rates with increasing number of cycles [4, 5, 47, 48]. For that reason, Duque et al. [3] enhanced the intergranular strain concept through the so-called "ISI" based on a similar mechanism previously proposed by Poblete [33]. This enhancement involves introducing a function that enables the model's strain rate of accumulation to evolve upon increasing number of cycles.

In this article, the coupled hydro-mechanical hypoplastic model for fine-grained soils by Wong and Mašín [51] is extended considering the following modifications: (1) the water retention curve (WRC) is replaced with a hysteretic void-ratio-dependent smoothed formulation proposed by Svoboda et al. [37] to predict the nonlinear relationship between suction and the degree of saturation; (2) the model is enhanced with ISI to adequately predict the accumulation rates of cyclic tests considering different suction levels; (3) a dependency of the ISI enhancement on the degree of saturation to account for partially saturated effects under cyclic loading. The extended model was thoroughly validated by comparing element test simulations using the reference and extended models with experimental results on a completely decomposed tuff (CDT) subjected to monotonic and cyclic loading at different suction levels reported by Ng et al. [27–30, 54]. The comparison between experimental measurements and numerical predictions suggests that the extended model is capable of capturing cyclic behavior under partially saturated conditions, while also conserving the predictive capabilities of the model for monotonic loading.

The structure of the subsequent sections is as follows: Sect. 2 presents a description of the reference soil constitutive model. Then, Sect. 3 presents the characteristics of the testing materials adopted for calibration and validation purposes. Section 4 presents the numerical implementation and element test simulations of the experimental tests. Finally, Sect. 5 provides the summary and conclusions of the article.

2 Description of the constitutive model

2.1 Background

The constitutive model proposed in this work has been developed within the basis of hypoplasticity, which corresponds to a family of constitutive models capable of modelling nonlinear soil behavior while considering the effects of barotropy and pyknotropy. The initial development of hypoplasticity started in Karlsruhe and was primarily focused on granular materials. For instance, the model by von Wolffersdorff [41] summarizes the work developed at that time. Later on, Mašín [16, 18] proposed an hypoplastic model for fine-grained soils combining the generalized hypoplastic principles with traditional critical state soil mechanics. The main idea behind hypoplasticity is to explain the material behavior trough a single nonlinear tensorial equation, linking the stress tensor rate $\dot{\boldsymbol{\sigma}}$ with the strain tensor rate $\dot{\boldsymbol{\varepsilon}}$. In its general form, it can be written as follows:

$$\dot{\boldsymbol{\sigma}} = f_s(\mathcal{L} : \dot{\boldsymbol{\varepsilon}} + f_d \boldsymbol{N} \|\dot{\boldsymbol{\varepsilon}}\|) \tag{1}$$

where $\dot{\boldsymbol{\sigma}}$ and $\dot{\boldsymbol{\varepsilon}}$ correspond to the stress rate and Euler stretching tensor, respectively, and $\mathcal{L}$ and $\boldsymbol{N}$ are fourth- and second-order hypoplastic constitutive tensors. In hypoplasticity, the stiffness of the model is generally control by the tensor $\mathcal{L}$, meanwhile strength and asymptotic states are ruled by the combination of both $\mathcal{L}$ and $\boldsymbol{N}$ [18]. f_d and f_s represent scalar factors for considering the effects of pyknotropy and barotropy. Several authors [9, 15, 26, 38, 42] have reported good predictive capabilities of hypoplastic models under medium and large strain amplitudes ($\| \Delta\boldsymbol{\varepsilon}\| < 10^{-3}$). However, some limitations of the model have been observed. Consequently, different enhancements have been proposed to account for the effects of soil behavior under various loading and environmental conditions. For instance, Nieumunis and Herle [31] enhanced the hypoplastic formulation to account for small strain stiffness effects by adding a state variable, the so-called "intergranular strain $\boldsymbol{\delta}$", to predict an increase in stiffness upon reversal loading. The model has also been extended to reproduce visco-plastic effects [11], stiffness

anisotropy [19], double-structure behavior [20] and thermo-hydro-mechanical effects [23], as well as the incorporation of partially saturated effects under small strain stiffness conditions [51]. Similarly, in this article, the coupled hydro-mechanical model by Wong and Mašín [51] was taken as a reference to further develop a coupled hydro-mechanical constitutive model for unsaturated fine-grained soils under monotonic and cyclic loading.

The development of the constitutive model has been carried out following a hierarchical methodology. The hierarchical development of the constitutive model offers the user practical advantages. One of them is that different components of the constitutive model can be activated or deactivated according to the soil behavior under matters. As an example, if addressing soil behavior under saturated and monotonic conditions, only five parameters from the basic hypoplastic model by Mašín [18] are required. In this way, the constitutive model can be employed for a wide range of conditions according to the user's needs, providing a simplified version for simpler problems without losing its predictive capabilities.

2.2 Features of the constitutive model

The hypoplastic constitutive model presented in this article has evolved from the previous coupled hydro-mechanical model for partially saturated soils predicting small strain stiffness, developed by Wong and Mašín [51]. This model is hereafter referred to as "HIS-unsat+BWRC". The base model incorporates various features of previously developed hypoplastic models for predicting soil behavior under different stress states, corresponding to the following:

- The base model predicts asymptotic state under large strain behavior, thanks to the explicit incorporation of an Asymptotic State Boundary Surface (ASBS). The ASBS represents all asymptotic states in the stress versus void ratio space. More details can be found in [18]. The asymptotic state boundary surface enables the prediction of the critical state and the isotropic asymptotic states. Additionally, the constitutive model incorporates the failure criterion proposed by Matsuoka and Nakai [25].

- Unsaturated mechanical effects are account for in the model formulation, following the previous work by Mašín and Khalili [22]. The model is defined in terms of the effective stress approach formulated by Khalili and Khabbaz [12], which allows the model to predict higher shear strength at higher suction magnitudes. The size of the ASBS is defined to be dependent on suction, as the increment in suction produces a soil response similar to an increase in over-consolidation ratio. For this purpose, the normal compression line of the model

is defined to be dependent on suction. In addition, the constitutive model predicts wetting-induced collapse, an effect observed during wetting of normally consolidated soils, and its influences diminishes as the over-consolidation ratio increases.

- The coupled hydro-mechanical behavior is governed by a hysteretical bi-linear water retention curve introduced in the model following the work by Mašín [17]. Thanks to the hysteretical properties of the WRC, the model can predict a different response between drying or wetting states. Additionally, the WRC is defined to be dependant on void ratio, influencing the coupling between the hydraulic and mechanical behavior [22].

- Small strain stiffness effects are predicted by means of the intergranular strain concept by Nieumunis and Herle [31]. For that purpose, information about the recent strain history is stored in a strain-type state variable, which enables the model to detect wether the material has been subjected to monotonic or reversal loading. The information given by the state variable allows the constitutive model to have higher stiffness upon loading reversal and a decrease in the accumulated strain.

In this paper, three extensions have been added to the reference model by Wong and Mašín [51] to adequately describe the behavior of unsaturated fine-grained soils under monotonic and cyclic loading:

- The water retention curve has been modified to include a smoothed formulation proposed by Svoboda et al. [37].

- The improvement of the intergranular strain concept developed by Duque et al. [3] was introduced in the model to predict the soil behavior under a large number of repetitive cycles (e.g. $N > 10$).

- The ISI concept was further extended to capture the dependency of strain accumulation rate on the degree of saturation for modeling the behavior of unsaturated soils under cyclic loading conditions.

Table 1 presents the new model parameters along with a brief summary of their meaning, calibration procedure and the reference model from which they were first proposed. A more detail explanation about the model parameters can be found in Appendix 3.

The following sections describe the main components of the reference and extended model.

2.2.1 Description of the hypoplastic model for fine-grained soils

The general rate equation of the model is given by:

Table 1 Model parameters, meaning, calibration procedure and reference model

Parameter	Units	Description	Useful test	Introduced by
φ_c	°	Critical state friction angle	Drained triaxial shear tests	[18]
λ^*	–	Slope of the normal compression line	Isotropic/oedometric compression tests	[18]
κ^*	–	Slope of the loading/reloading line	Isotropic/oedometric compression tests	[18]
N	–	Reference void ratio	Isotropic/oedometric compression tests	[18]
v_{pp}	–	Poisson ratio	Undrained triaxial shear tests	[18]
n_s	–	Dependency of the normal compression line on suction	Suction controlled isotropic/oedometric tests	[22]
l_s	–	Dependency of the loading/reloading line on suction	Suction controlled isotropic/oedometric tests	[22]
m	–	Rate at which the susceptibility of the soil structure to collapse decreases with increasing distance from the SBS	Wetting tests on slightly over-consolidated soils	[22]
s_{en0}	kPa	Reference air entry value of suction for the reference void ratio e_0	WRC tests	[17]
e_0	–	Reference void ratio for s_{en_0} and λ_{p0}	WRC tests	[17]
λ_{p0}	–	Slope of the water retention curve in the $\ln(S_r)$ versus $\ln(s_e/s)$ plane	WRC tests	[17]
a_e	–	Ratio of air expulsion and air entry value of suction	WRC tests	[17]
γ	–	Effective stress parameter, its value is set to 0.55 as suggested by Khalili and Khabbaz [12]	–	[12]
A_g	–	Transversal very small strain shear modulus G_{tp0} of saturated soil for the reference stress $p_r = 1$ kPa	Measurements of shear wave velocity at very small strains	[52]
n_g	–	Dependency of the transversal very small strain shear modulus G_{tp0} of saturated soil on mean effective stress p	Measurements of shear wave velocity at very small strains	[52]
m_g	-	Dependency of the transversal very small strain shear modulus G_{tp0} of saturated soil on void ratio	Measurements of shear wave velocity at very small strains	[52]
k_g	–	Dependency of the small strain shear modulus on the degree of saturation S_r	Measurements of shear wave velocity at very small strains	[52]
R	–	Size of the very small-strain elastic range (intergranular strain concept for small strain stiffness)	Triaxial shear experiments	[31]
r_m	–	Controls the dependency of the size of the elastic range on the degree of saturation	Triaxial shear experiments	[51]
β_r	–	Controls the strain amplitude at which small strain effects are active	Triaxial shear experiments	[31]
m_{rat}	–	Controls the ratio of very-small-strain shear modulus upon changes of strain path direction	Triaxial shear experiments	[31]
χ_{0g}	–	Minimum value of stiffness decay on the first cycles	Undrained cyclic triaxial test ($N \leq 5$)	[3]
χ_{max}	–	Rate of accumulation after a large number of repetitive cycles ($N \geq 10$) in saturated conditions	Drained/undrained cyclic triaxial tests	[3]
C_Ω	–	Rate at which the strain accumulation rates changes the exponent χ_g from χ_{g0} to χ_{max}	Rate of pore water pressure accumulation from undrained triaxial tests	[3]
γ_χ	–	Controls the accumulation of strains and excess pore pressures due to cyclic loading	Cyclic simple shear or triaxial tests	[43]
ϑ_w	–	Controls the dependency of the rate of accumulation at small strain amplitudes on the degree of saturation S_r	Cyclic constant water/suction controlled triaxial tests	This model

$$\dot{\boldsymbol{\sigma}} = f_s(\mathcal{L} : \dot{\boldsymbol{\varepsilon}} + f_d \mathbf{N} \|\dot{\boldsymbol{\varepsilon}}\|) + f_u \mathbf{H}_s \tag{2}$$

where $\dot{\boldsymbol{\sigma}}$ represents the rate of effective stress (for geometric nonlinearities due to large deformations, the Jaumann stress rate can be adopted instead), $\mathcal{L}$ is the fourth-order stiffness tensor, $\mathbf{N}$ is the second-order hypoplastic tensor, $\dot{\boldsymbol{\varepsilon}}$ is the Euler stretching tensor (using the simplified assumption of linear kinematics, it is equal to the rate of strain), $\|\dot{\boldsymbol{\varepsilon}}\|$ is the Euclidean norm of $\dot{\boldsymbol{\varepsilon}}$ with $\|\dot{\boldsymbol{\varepsilon}}\| = \sqrt{\dot{\boldsymbol{\varepsilon}} : \dot{\boldsymbol{\varepsilon}}}$,

and $\mathbf{H_s}$ is a second-order tensor incorporated into the model to reproduce wetting-induced collapse. The factors f_s and f_d are introduced to account for the effects of barotropy and pyknotropy, respectively. In addition, the scalar f_u vanishes the reproduction of wetting-induced collapse for increasing over-consolidation ratios. Their mathematical definition can be found in Appendix 2. The constitutive model has been defined in terms of the effective stress $\boldsymbol{\sigma}$, that follows from the relation proposed by Khalili and Khabbaz [12] as:

$$\boldsymbol{\sigma} = \boldsymbol{\sigma}^{\text{net}} - \boldsymbol{1}\chi s \tag{3}$$

where s represents suction, $\boldsymbol{\sigma}^{\text{net}}$ corresponds to the net stress and χ is defined as:

$$\chi = \begin{cases} \left(\dfrac{s_e}{s}\right)^{\gamma}, & \text{for } s > s_e \\ 1, & \text{for } s < s_e \end{cases} \tag{4}$$

s_e represents the air entry suction as depicted in Fig. 1. The value of γ was selected based on the previous study by Khalili and Khabbaz [12], who after evaluating shear strength data of several types of soils (14), concluded that a value of $\gamma = 0.55$ can properly reproduced the relationship between the effective stress parameter (χ) and the ratio of suction and the air entry value (s/s_{en}). Nevertheless, advanced-users of the constitutive model could adjust this data based on experimental results of shear strength data. By using a Brooks and Corey-type relation for the WRC $S_r = (s_e/s)^{\lambda_p}$, Eq. (4) can be rewritten as:

$$\chi = S_r^{(\gamma/\lambda_p)} \tag{5}$$

In this way, the effective stress rate of the model can be expressed as suggested by Wong and Mašín[51] as:

$$\begin{aligned} \dot{\boldsymbol{\sigma}} &= \dot{\boldsymbol{\sigma}}^{\text{net}} - \boldsymbol{1}\left[\frac{\partial(\chi s)}{\partial t}\right] \\ &= \dot{\boldsymbol{\sigma}}^{\text{net}} - \boldsymbol{1}\left[\frac{\partial(\chi s)}{\partial s}\dot{s} + \frac{\partial(\chi s)}{\partial e}\dot{e}\right] \end{aligned} \tag{6}$$

where

$$\frac{\partial(\chi s)}{\partial s} = (1 - \gamma r_{\lambda\text{scan}})\chi \tag{7}$$

and for $s > s_e$

$$\frac{\partial(\chi s)}{\partial e} = -\frac{s\gamma^2}{e\lambda_{\text{psu}}}\left(\frac{s_{\text{en}}}{s}\right)^{\gamma} \tag{8}$$

otherwise $\partial(\chi s)/\partial e = 0$

Combining Eqs. 7 and 8 into Eq. 2 by transferring the term $\partial(\chi s)/\partial e$ to its right-hand side and including it in a modified $\mathcal{L}$ tensor denoted as $\mathcal{L}^{HM}$ to indicate unsaturated conditions, the hypoplastic rate equation can be rewritten for unsaturated conditions ($S_r < 1$), as:

$$\dot{\boldsymbol{\sigma}}^{\text{net}} - \boldsymbol{1}(1 - \gamma r_{\lambda\text{scan}})\chi\dot{s} = f_s(\mathcal{L}^{HM} : \dot{\boldsymbol{\varepsilon}} + f_d\mathbf{N}\|\dot{\boldsymbol{\varepsilon}}\|) + f_u\mathbf{H_s} \tag{9}$$

where

$$\mathcal{L}^{HM} = \mathcal{L} - \frac{s(1+e)\gamma^2}{f_s e\lambda_{\text{psu}}}\left(\frac{s_{\text{en}}}{s}\right)^{\gamma}\boldsymbol{1} \otimes \boldsymbol{1} \tag{10}$$

Meanwhile, for saturated conditions ($S_r = 1$), Eq. 9, simplifies to

$$\dot{\boldsymbol{\sigma}}^{\text{net}} - \boldsymbol{1}\dot{s} = f_s(\mathcal{L} : \dot{\boldsymbol{\varepsilon}} + f_d\mathbf{N}\|\dot{\boldsymbol{\varepsilon}}\|) \tag{11}$$

To include the mechanical effects of partial saturation, the size of asymptotic state boundary surface of the model is defined to be suction dependent. For that purpose, the normal compression line is defined to be depending on suction according to the following:

$$\ln(1+e) = N(s) - \lambda^*(s)\ln\frac{p}{p_r} \tag{12}$$

where $N(s)$ and $\lambda^*(s)$ are defined as:

$$N(s) = N + n_s\left\langle \ln\left(\frac{s}{s_e}\right)\right\rangle \tag{13}$$

$$\lambda^*(s) = \lambda^* + l_s\left\langle \ln\left(\frac{s}{s_e}\right)\right\rangle \tag{14}$$

where N and λ^* correspond to basic parameters for saturated conditions as described by Mašín [18]. Meanwhile, l_s and n_s are additional parameters introduced by Mašín and Khalili [22] to account for the influence of suction s on the normal compression line. In addition, a second order tensor $\mathbf{H_s}$ is included into the basic hypoplastic equation for avoiding super-passing the asymptotic state boundary surface during wetting. Its definition is given according to
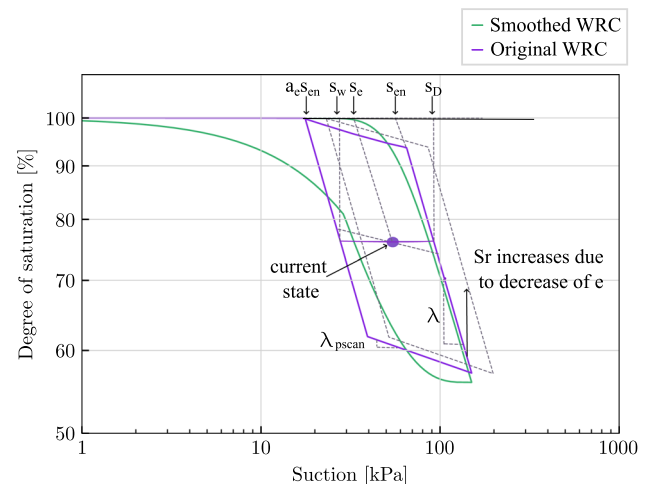

Fig. 1 Comparison between the original and the smoothed water retention curves

$$\mathbf{H}_s = -\frac{c_i r_{\lambda\text{scan}}\boldsymbol{\sigma}}{s\lambda^*(s)}\left(n_s - l_s \ln\frac{p_e}{p_r}\right)\langle -\dot{s}\rangle \tag{15}$$

where p_e represents the Hvorslev equivalent pressure, defined as the mean effective stress at the normal compression line for the current suction and void ratio values, and c_i corresponds to a factor introduced by Mašín and Khalili [23] to enhance the prediction of over-consolidated states. The definition of this factor can be found in Appendix 2. The factor $r_{\lambda scan}$ will be introduced later in Sect. 2.2.2.

2.2.2 Description of the hysteretic water retention response

For controlling the hydraulic response of the constitutive model, the reference model presented by Wong and Mašín [51] employed a hysteretical bi-linear water retention curve based on the formulation by Brooks et al. [2]. However, real soils exhibit a nonlinear dependency between the degree of saturation S_r and suction s. Thus, in the extended version of the constitutive model, a hysteretic water retention curve defined by a smoothed function formulated by Svoboda et al. [37] has been incorporated to predict hysteretical hydraulic behavior. An advantage of this formulation is its improvement of numerical performance thanks to the smooth derivatives $\partial S_r/\partial s$ at the intersections of the main wetting/drying curves with the scanning curves and at the air entry/expulsion suction value. Additionally, this smoothed formulation is in agreement with the inherent nonlinearity of the hypoplastic framework. The outline of the hydraulic model is presented in Fig. 1. The complete water retention curve is defined according to:

$$S_r = \begin{cases} 1, & \text{for } s \le a_e s_{\text{en}} \\ \left(\frac{s_e}{s}\right)^{\lambda_p}, & \text{for } s > a_e s_{\text{en}} \end{cases} \tag{16}$$

where a_e is a parameter that indicates the ratio between the air expulsion and the air entry value. λ_p corresponds to the slope of the main drying or wetting curve and it is defined to be dependent on void ratio according to the following expression:

$$\lambda_p = \frac{\gamma}{\ln\chi_0}\ln\left[\left(\chi_0^{\frac{\lambda_{p0}}{\gamma}} - \chi_0\right)\left(\frac{e}{e_0}\right)^{(\gamma-1)} + \chi_0\right] \tag{17}$$

where $\chi_0 = \left(\frac{s_{\text{en0}}}{s}\right)^{\gamma}$ and λ_{p0}, s_{en0} and e_0 are model parameters that represent reference values of the slope of the main drying or wetting curve, air entry value and reference void ratio, respectively. In the reference model, the ratio between the slope of the of the main drying or wetting curve and the scanning curve slope (λ_{pscan}) defined in the $\ln s$ versus $\ln S_r$ plane was given by factor r_λ, as:

$$r_\lambda = \begin{cases} 1 & \text{for } s = s_D \text{ and } \dot{s} > 0 \\ 1 & \text{for } s = a_e s_D \text{ and } \dot{s} < 0 \\ \dfrac{\lambda_{\text{pscan}}}{\lambda_p} & \text{otherwise} \end{cases} \tag{18}$$

Svoboda et al. [37] used the definition of r_λ to introduce a smoothed transition of the scanning curves between the main drying and wetting curves. The formulation incorporates three default parameters denoted as $p_{\text{scan}} = 3$, $S_{\text{lim}} = 0.5$, and $p_{\text{wett}} = 1.1$, which are intended to be hidden from the user. However, the values can be adjusted if it is necessary depending on the soil properties and results of water retention curves. More information related to the influence of each parameter can be found in Svoboda et al. [37]. The redefinition of r_λ is given according to:

$$r_\lambda = \begin{cases} 0 & \text{for} & s < a_e s_{\text{en}} \text{ and } \dot{s} > 0 \\ \left(\dfrac{1 - S_r}{1 - S_{\text{lim}}}\right)^{p_{\text{wett}}} & \text{for} & S_r > S_{\text{lim}} \text{ and } \dot{s} < 0 \\ \left(f_{\text{scan}}^{p_{\text{scan}}}\right) & \text{otherwise} \end{cases} \tag{19}$$

The smoothed formulation includes the factor f_{scan}, defined as follows:

$$f_{\text{scan}} = \begin{cases} a_{\text{scan}} & \text{for } \dot{s} > 0 \\ 1 - a_{\text{scan}} & \text{for } \dot{s} < 0 \end{cases} \tag{20}$$

where a_{scan} corresponds to a state variable employed for modeling hysteretical hydraulic behavior. This variable evolves between the values of 0 when the current state is on the main wetting curve, to 1 when the state lies at the main drying curve, such that:

$$a_{\text{scan}} = \frac{s - s_W}{s_D - s_W} \tag{21}$$

The meaning of s_W and s_D is depicted in Fig. 1. The rate of a_{scan} is defined as:

$$\dot{a}_{\text{scan}} = \frac{1 - r_{\lambda\text{scan}}}{s_D(1 - a_e)}\dot{s} \tag{22}$$

The factor $r_{\lambda\text{scan}}$ has been introduced into the model to control the evolution of the state variable a_{scan}, which remains equal to zero even at states where Eq. 18 yields $r_\lambda = [(1 - S_r)/(1 - S_{\text{lim}})]^{p_{\text{wett}}}$. The definition of $r_{\lambda\text{scan}}$ is given as:

$$r_{\lambda\text{scan}} = \begin{cases} 0 & \text{for } s < a_e s_{\text{en}} \text{ and } \dot{s} > 0 \\ f_{\text{scan}}^{p_{\text{scan}}} & \text{otherwise} \end{cases} \tag{23}$$

The air entry value is represented by s_{en} and it is considered a state variable that depends on void ratio. Its evolution equation is accounted through the following relation:

$$\dot{s}_{en} = -\frac{\gamma s_{e_n}}{e\lambda_{psu}}\dot{e} \tag{24}$$

The definition of λ_{psu} can be found in Appendix 2 and more details about its meaning are given in [52]. Lastly, the meaning of s_e is shown in Fig. 1. Its calculation is given according to:

$$s_e = s_{en}(a_e + a_{scan} - a_e a_{scan}) \tag{25}$$

Figure 1 illustrates a comparison between the previous and the updated versions of the water retention curve. As is evident, the updated model is able to reproduce the non-linear dependency between suction and the degree of saturation, while maintaining the main drying and wetting curves as asymptotic targets.

2.2.3 Description of the intergranular strain extension

The base formulation of the constitutive model considered small strain stiffness effects through the intergranular strain (IS) concept, developed by Niemunis and Herle [31], including a modified feature for partially saturated effects. The intergranular strain concept assumes that the strain results from the deformation of the intergranular interface layer and from the rearrangement of the skeleton [31]. The deformation of the interface is denoted as intergranular strain $\boldsymbol{\delta}$, and it is defined as a strain-type (second ranked) tensor, whose normalized magnitude is given as:

$$\rho = \frac{\|\boldsymbol{\delta}\|}{R(S_r)} \tag{26}$$

where $R(S_r)$ corresponds to the maximum Euclidean norm of $\boldsymbol{\delta}$. Wong and Mašín [51] formulated the size of the elastic range $R(S_r)$ to be dependent on the degree of saturation by evaluating the model using experimental data on small strain stiffness of partially saturated soils, its dependency can be described by the following expression:

$$R(S_r) = R - \frac{r_m}{\lambda_p}\ln S_r \tag{27}$$

where R, r_m and λ_p are model parameters. r_m is a model parameter that controls the dependency of the elastic range on the degree of saturation (S_r). It can be calibrated using stiffness degradation curves at different degree of saturation. Time derivative of $\dot{R}(S_r)$ gives

$$\dot{R}(S_r) = r_m\left(-\frac{\dot{S}_r}{S_r\lambda_p} + \frac{\gamma}{e\lambda_{psu}}\dot{e}\right) \tag{28}$$

Considering the dependency of the elastic range on the degree of saturation and void ratio, the original evolution equation of the intergranular strain tensor by Niemunis and Herle [31] was modified by Wong and Mašín [51] as follows:

$$\dot{\boldsymbol{\delta}} = \begin{cases} \left(\mathcal{I} - \hat{\boldsymbol{\delta}} \otimes \hat{\boldsymbol{\delta}}\rho^{\beta_r}\right) : \dot{\boldsymbol{\varepsilon}} + \boldsymbol{\delta}\dfrac{\langle\dot{R}(S_r)\rangle}{R(S_r)} & \text{for } \hat{\boldsymbol{\delta}} : \dot{\boldsymbol{\varepsilon}} > 0 \\ \dot{\boldsymbol{\varepsilon}} & \text{for } \hat{\boldsymbol{\delta}} : \dot{\boldsymbol{\varepsilon}} \le 0 \end{cases} \tag{29}$$

where β_r corresponds to a soil parameter that controls the stiffness decay in the small strain range. The direction of the intergranular strain tensor is given as

$$\hat{\boldsymbol{\delta}} = \begin{cases} \dfrac{\boldsymbol{\delta}}{\|\boldsymbol{\delta}\|} & \text{for } \boldsymbol{\delta} \neq \boldsymbol{0} \\ \boldsymbol{0} & \text{for } \boldsymbol{\delta} = \boldsymbol{0} \end{cases} \tag{30}$$

This approach enables to capture the influence of both recent stress and suction history on the evolution of the intergranular strain. This is because changes in both stress and suction results in soil deformation, subsequently causing changes in $\boldsymbol{\delta}$. The overall stress–strain relation can be reformulated as follows:

$$\dot{\boldsymbol{\sigma}} = \mathcal{M} : \dot{\boldsymbol{\varepsilon}} + f_u\boldsymbol{H}_s \tag{31}$$

where $\mathcal{M}$ represents the tangent stiffness and its calculation is made by using the following interpolation between the hypoplastic tensors $\mathcal{L}$ and $\mathbf{N}$

$$\mathcal{M} = [\rho^{\chi_g}m_T + (1 - \rho^{\chi_g})m_R]f_s\mathcal{L} \\ + \begin{cases} \rho^{\chi_g}(1 - m_T)f_s\mathcal{L} : \hat{\boldsymbol{\delta}} \otimes \hat{\boldsymbol{\delta}} + \rho^{\chi_g}f_sf_d\mathbf{N}\hat{\boldsymbol{\delta}} & \text{for } \hat{\boldsymbol{\delta}} : \dot{\boldsymbol{\varepsilon}} > 0 \\ \rho^{\chi_g}(m_R - m_T)f_s\mathcal{L} : \hat{\boldsymbol{\delta}} \otimes \hat{\boldsymbol{\delta}} & \text{for } \hat{\boldsymbol{\delta}} : \dot{\boldsymbol{\varepsilon}} \le 0 \end{cases} \tag{32}$$

The variable m_T is defined as $m_T = m_{rat}m_R$, where $m_{rat} \le 1$ is a model parameter. In addition, the variable m_R controls the very small strain stiffness magnitude and is given as:

$$m_R = G_{tp0}\frac{4A_m\alpha_g}{9p\alpha_e}\left(\frac{\lambda_{act}^*\kappa^*}{\lambda_{act}^* + \kappa^*}\right)\frac{1}{1 - v_{pp} - 2\frac{\alpha_E}{\alpha_v^2}v_{pp}^2} \tag{33}$$

where

$$G_{tp0} = p_rA_g\left(\frac{p}{p_r}\right)^{n_g}e^{(-m_g)}S_r^{(-k_g/\lambda_p)} \tag{34}$$

Stiffness anisotropy is also incorporated into the model. Here, the subscripts "t" and "p" correspond to the transverse and in-plane directions, respectively, with respect the plane of transversal isotropy. Additional details can be found in Mašín [24]. The definitions of other variables of Eq. (33) are provided in Appendix 2. The formulation of the shear modulus at very small strains, G_{tp0}, presented in Eq. 34, was developed by Wong et al. [52] after analyzing the very small strain behavior of four different fine-grained soils in unsaturated conditions. n_g, m_g and k_g are material parameters for controlling the dependency of G_{tp0} on the mean effective stress, void ratio and degree of saturation,

respectively, and p_r corresponds to a reference pressure $p_r = 1.0$ kPa.

Experimental observations have indicated that as the number of cycles of small strain amplitudes ($\|\Delta\epsilon\| < 10^{-3}$) increases, the rate of strain accumulation reduces [4, 5, 47, 48, 50]. This observation is not replicated by the intergranular strain model, as noted by various authors (e.g., [9, 33, 33, 40, 43]). Therefore, the base model was enhanced by integrating the improved intergranular strain concept proposed by Duque et al. [3], developed upon the observations by Poblete et al. [33] and Wegener and Herle [43]. The main aim of the ISI enhancement is to predict the dependency of the strain accumulation rate on the previously performed cycles. To achieve this, the parameter χ_g in the intergranular strain concept is modified to become a function that evolves according to the number of cycles of loading performed, utilizing a new internal variable Ω. This variable ranges from one ($\Omega \to 1$) when the intergranular strain is not mobilized ($\rho \approx 0$), and gradually decreases to zero during monotonic paths or when reaching large strain amplitudes. The equation governing its evolution is presented as follows:

$$\dot{\Omega} = C_\Omega(1 - \rho^{\gamma_g} - \Omega)\|\dot{\boldsymbol{\varepsilon}}\| \tag{35}$$

where C_Ω represents a parameter that governs the rate of reduction in the strain accumulation rate. Subsequently, γ_g is used to replace the exponent χ_g in the term $\rho^{\chi_g}\mathbf{N}\hat{\boldsymbol{\delta}}$ [refer to Eq. (32)], employing the function $\gamma_g = \gamma_\chi\chi_g$ instead. This term is responsible for controlling the hypoplastic stiffness during unloading. Notably, γ_χ corresponds to a new model parameter, and the value of χ_g is defined as follows:

$$\chi_g = \chi_{g0} + \Omega(\chi_{max} - \chi_{g0}) \tag{36}$$

In this manner, the value of χ_g transitions from a minimum value $\chi_g = \chi_{g0}$ when $\Omega = 0$ (monotonic loading) and achieves its maximum $\chi_g = \chi$max when $\Omega = 1$ upon several cyclic episodes.

2.2.4 Incorporation of the dependency on the degree of saturation to the ISI concept

Despite the fact that the experimental data available in the literature concerning partial saturation on cyclic loading effects is scarce, most of the authors have reported the following findings: a) an increase in the yielding stress with the increase in suction (suction-induced hardening), b) an increase in stiffness with suction, resulting in smaller volumetric and axial strains with increasing suction and slower accumulation. Based on these noted trends and upon a more detailed analysis of the constant water triaxial experiments conducted by Ng and Zhou [30, 54] under different suction levels, it was found that the base numerical model "HIS-unsat+BWRC" failed to reproduce the increase in stiffness attributed to suction effects, using a single set of parameters for each suction level. Consequently, given that the function χ_g governs both the stiffness degradation of the material and the strain accumulation upon cyclic loading, an exponential dependency of the parameter χ_{max} [part of Eq. (36)] and the degree of saturation is proposed, as indicated by the following expression:

$$\chi_{max}(S_r) = \chi_{max}S_r^{\vartheta_w} \tag{37}$$

where χ_{max} corresponds to the value of the parameter under saturated conditions, and ϑ_w represents a new parameter calibrated according to the change in strain accumulation during cyclic tests conducted under different saturation conditions. This equation was derived through a two-step process. Initially, the value of χ_{max} was calibrated for different levels of suction. Subsequently, a numerical interpolation was carried out using the optimized χ_{max} values corresponding to each suction level. Further insights into this process are available in Appendix 4, which presents the outcomes of the optimized calibration and provides a detailed explanation of the procedure followed. The complete mathematical formulation of the model is presented in Tables 7, 8, 9 and 10 (See Appendix 2). Furthermore, Appendix 5 shows a sensitivity analysis to illustrate the effect of certain parameters from the proposed model associated with the improvement of the intergranular strain.

3 Test material and experiments

The performance of the constitutive model was assessed using experimental data available in the literature for a completely decomposed tuff (CDT) from Hong-Kong, classified as clayey silt (ML) according to the Unified Soil Classification System. The material was originally sampled from a deep excavation site at Fanling, Hong Kong. It was described as yellowish-brown, slightly plastic, with a very small percentage of fine and coarse sand. The index properties of the material are as follows: $w_L = 43\%$, $w_P = 29\%$, $G_s = 2.73$. Additional information about the tested soil can be found in Ng and Yung [29].

The selected experimental tests encompass both monotonic and cyclic loading conditions to ensure that the new features of the model do not impact its capabilities under monotonic loading. To calibrate the model's compression law and parameters associated with unsaturated mechanical behavior $\{\lambda^*, \kappa^*, N, l_s, \text{ and } n_s\}$, suction-controlled isotropic compression tests performed by Ng and Yung [29] were

selected. These tests were conducted at four suction values $s = \{0, 50, 100, 200\}$ kPa. Drying and wetting tests carried out under two different confining pressures $p^{\text{net}} = \{110, 300\}$ kPa, as reported by Ng and Xu [28], were employed to calibrate parameters related to water retention behavior $\{s_{\text{en}0}, e_0, \lambda_{p0}, a_e\}$. Additionally, triaxial tests under constant p^{net} conditions with varying wetting and drying paths [27] were considered for calibrating parameters related to very small strain stiffness effects $\{G_{tp0}, A_g, m_g, n_g, k_g, m_{\text{rat}}\}$. Furthermore, the parameters influencing the enhancement of the intergranular strain concept $\{R, \beta_r, \chi_{g0}, \chi_{\text{max}}, r_m, C_\Omega, \gamma_\chi, \vartheta_w\}$ were calibrated using constant water content cyclic triaxial tests at three suction magnitudes $s = \{0, 30, 60\}$ kPa conducted by Ng et al. [30, 54]. A summary of the testing program, including the suction magnitude, initial mean net stress, initial deviatoric stress, amplitude of deviatoric stress, and initial void ratio in the experimental program, is presented in Table 2.

4 Numerical implementation and element test simulations with the proposed model

The model's capabilities to reproduce monotonic and cyclic behavior of partially saturated soils were evaluated through simulations of element tests. The numerical model was implemented as a subroutine in the freely accessible in-house software TRIAX [21], which enables users to compute various laboratory element tests and seamlessly integrate the constitutive model into open-source finite element programs, such as SIFEL [14] and OPENGEOSYS [13] through the interface called "generalmod". Its implementation followed the procedure by Janda and Mašín [10].

The time integration of the constitutive model used in this paper employed a simple Forward-Euler scheme, with very small strain increments. Due to the high nonlinearity of the constitutive model, different values of strain increments sizes were carefully considered until finding a value that assures convergence and avoids accumulation of numerical errors. The final value that was selected was ($\Delta\varepsilon \approx 10^{-5}$), assuring a strain increment small enough to avoid accumulation of numerical errors that would influence the results of the numerical simulations. This type of assessment is suggested to be performed, specially when simulating cyclic loading, to avoid accumulation of numerical errors.

Three versions of the constitutive model were used for the numerical simulations. The first version corresponds to the reference base model with the material calibration proposed by Wong and Mašín [51]. This version will be addressed herein as "HIS-unsat+BWRC". The second version pertains to the reference base model, incorporating a modification of the water retention curve using the smoothed formulation by Svoboda et al. [37], along with a re-calibrated set of parameters based on the experimental results from constant water content cyclic triaxial tests. In this study, it will be denoted to as "HIS-unsat+SWRC". The third version of the constitutive model incorporates all the modifications explained in Sect. 2.2, including the smoothed water retention curve and the improvement of intergranular strain concept (ISI) with a dependency on the degree of saturation. This version will be abbreviated as "HISI-unsat+SWRC" herein. Table 3 provides a brief explanation of each model version, including details about the type of water retention curve, the calibrated parameter set, and whether the original intergranular strain concept or the improved formulation is employed. Additionally, Tables 4, 5, and 6 summarize the calibrated parameter values utilized in the numerical simulations for each version of the model.

The element test simulations were conducted with the complete stress history as per the experimental procedure. The void ratio was initialized in each simulation using the documented experimental values provided in Table 2. To replicate the effects of the sample preparation method (e.g., one-dimensional compression), the intergranular strain tensor was initialized under fully mobilized oedometric conditions as $\delta_{11} = -R(S_r)$. The initial value of the state variable a_{scan} depends on the suction history of the soil. For instance, it is initialized equal to 1.0 for simulations where the soil was previously dried, or equal to 0 when wetting was performed before simulation. The initial value of the state variable s_{en} is calculated by numerical integration of Eq. 24 from the value of e_0 to the initial void ratio. Additionally, the state variable Ω was initialized equal to 0 in all cases.

4.1 Water retention behavior

Two drying and wetting tests at two different constant mean net stresses, $p^{\text{net}} = 110$ kPa and $p^{\text{net}} = 300$ kPa, were taken from Ng et al. [28] to calibrate the parameters of the model controlling the water retention behavior $\{s_{\text{en}0}, a_e, e_0, \lambda_p\}$. The experiments were performed using compacted samples with an initial suction magnitude of 50 kPa. Subsequently, the samples were wet to achieve a suction of 0 kPa until reaching equilibrium. The samples were then dried to a suction value of 250 kPa and subsequently wet again to a final suction of $s = 0$ kPa. Suction-controlled conditions were employed in the element test and the complete stress history was reproduced in the numerical simulations.

Table 2 Summary of the experimental tests on CDT used for numerical simulations

Test name	s (kPa)	p_0 (kPa)	q_0 (kPa)	q^{amp} (kPa)	e_0 (–)	Reference (–)
ICS0[†]	0	110	–	–	0.632	[29]
ICS50[†]	50	110	–	–	0.656	
ICS100[†]	100	110	–	–	0.626	
ICS200[†]	200	110	–	–	0.628	
WRC110[‡]	0–250–0	110	–	–	0.637	[28]
WRC300[‡]	0–250–0	300	–	–	0.647	
CPTW°	95–1	100	0	–	0.568	[27]
CPTD1°	95–150	100	0	–	0.568	
CPTD2°	95–300	100	0	–	0.568	
CPTDWC1°	95–300–150	100	0	–	0.568	
CPTDWC2°	95–300–150–180–150	100	0	–	0.568	
CPTDWC3°	95–300–150–250–150	100	0	–	0.568	
CPTP110°	95–300–150–50–150	110	0	–	0.568	
CPTP200°	95–300–150–50–150	200	0	–	0.568	
CWTs0*	0	30	35	75	0.573	[30, 54]
CWTs30*	30	30	35	75	0.573	
CWTs60*	60	30	35	75	0.573	

[†]Suction controlled isotropic tests

[‡]Wetting and drying tests at constant confining pressure

°Suction controlled constant p triaxial tests

*Constant water cyclic triaxial tests

Table 3 Features of the versions of the constitutive model that were used for the numerical simulations

Model name	Type of WRC	Calibration	Small strain stiffness effects
HIS-unsat+BWRC	Bi-linear water retention curve	As proposed by Wong and Mašín [51]. See Table 4	Intergranular strain
HIS-unsat+SWRC	Smoothed water retention curve	Proposed in this paper. See Table 5	Intergranular strain
HISI-unsat+SWRC	Smoothed water retention curve	Proposed in this paper. See Table 6	ISI+ S_r dependency

unsat+SWRC" lies in its ability to describe the nonlinear relationship between the degree of saturation (S_r) and suction. This enhancement enables the model to achieve more realistic predictions in accordance with experimental evidence. Moreover, the smoothed formulation aligns better with the inherent nonlinearity definition of the constitutive model, thereby enhancing model performance in finite element simulations and avoiding convergence errors caused by numerical discontinuities.

The comparison between the experimental and numerical simulation results using the base model "HIS-unsat+BWRC", and the new formulation "HISI-unsat+SWRC" is presented in Fig. 2. The response using "HIS-unsat+BWRC" was excluded because it yields the same response as "HISI-unsat+SWRC" for this test type. As shown, both models successfully capture the hysteretic water retention behavior of the soil. Furthermore, both models replicate the dependency of the water retention curve on the void ratio, with the predicted degree of saturation decreasing as net confining pressure increases and the slope of the main drying and wetting curves steepens. Nevertheless, the experimental results indicated a stronger dependency. Additionally, the results reveal that the primary advantage of the new formulation "HISI-

Table 4 Parameters for completely decomposed tuff as calibrated by Wong and Mašín [51] used for HIS-unsat+BWRC

Type of behavior	Parameters					
Basic hypoplasticity	φ_c	λ^*	κ^*	N	v_{pp}	α_G
	35°	0.053	0.005	0.76	0.25	1
Unsaturated mechanical effects	n_s	l_s	m			
	0	0	(n/r)			
Water retention behavior	s_{en0}	e_0	λ_{p0}	a_e		
	67 kPa	0.568	0.6	0.5		
Very small strain stiffness effects	A_g	n_g	m_g	k_g		
	4220	0.55	0.9	0.2		
Intergranular strain	R	β_r	χ_g	m_{rat}	r_m	
	0.0001	2	1	1	8×10^{-5}	

Table 5 Recalibrated parameters for completely decomposed tuff used for HIS-unsat+SWRC

Type of behavior	Parameters					
Basic hypoplasticity	φ_c	λ^*	κ^*	N	v_{pp}	α_G
	35°	0.054	0.005	0.72	0.3	1.0
Unsaturated mechanical effects	n_s	l_s	m			
	0.035	0.0001	(n/r)			
Water retention behavior	s_{en0}	e_0	λ_{p0}	a_e		
	58 kPa	0.568	0.6	0.5		
Very small strain stiffness effects	A_g	n_g	m_g	k_g		
	4220	0.55	0.7	0.18		
Intergranular strain	R	β_r	χ_g	m_{rat}	r_m	
	0.0002	0.06	0.45	1.0	1×10^{-5}	

Table 6 Recalibrated parameters for completely decomposed tuff used for HISI-unsat+SWRC

Type of behavior	Parameters								
Basic hypoplasticity	φ_c	λ^*	κ^*	N	v_{pp}	α_G			
	35°	0.054	0.005	0.72	0.3	1			
Unsaturated mechanical effects	n_s	l_s	m						
	0.035	0.0001	(n/r)						
Water retention behavior	s_{en0}	e_0	λ_{p0}	a_e					
	58 kPa	0.568	0.6	0.5					
Very small strain stiffness effects	A_g	n_g	m_g	k_g					
	4220	0.55	0.7	0.18					
ISI	R	β_r	χ_{g0}	χ_{max}	C_Ω	γ_χ	m_{rat}	r_m	ϑ_w
	0.0002	0.06	0.15	0.31	30	7.0	1.0	1×10^{-5}	0.54

Table 7 Constitutive relations related to the very small strain stiffness shear modulus G_{tp0}

$$G_{tp0} = p_r A_g \left(\frac{p}{p_r}\right)^{n_g} e^{(-m_g)} S_r^{(-k_g/\lambda_p)}$$

$$m_R = G_{tp0} \frac{4 A_m \alpha_g}{9 p \alpha_e} \left(\frac{\lambda_{act}^* \kappa^*}{\lambda_{act}^* + \kappa^*}\right) \frac{1}{1 - v_{pp} - 2\frac{\alpha_E}{\alpha_v^2} v_{pp}^2}$$

$$m_T = m_R m_{rat}$$

$$A_m = v_{pp}^2 \left(\frac{4\alpha_E}{\alpha_v} - 2\alpha_E^2 + 2\frac{\alpha_E^2}{\alpha_v^2} - 1\right) + v_{pp}\left(\frac{4\alpha_E}{\alpha_v} + 2\alpha_E\right) + 2\alpha_E + 1$$

4.2 Suction controlled isotropic compression tests

The compressibility characteristics were defined to replicate the experimental results by Ng and Yung [29] from suction-controlled isotropic compression tests conducted at four distinct suction values $s = \{0, 50, 100, 200\}$ kPa. The simulations were performed by reproducing the full stress history followed in the experimental tests, which encompassed the following steps: initially, the samples were prepared using one-dimensional compaction with an initial suction value of 50 kPa. Subsequently, the desired suction value was applied to each sample. Finally, the samples underwent compression under isotropic conditions. Additional details about the experimental program can be found in the study by Ng and Yung [29].

The results of both the experimental tests and the numerical simulations are presented in Fig. 3. Firstly, it is evident that the model accurately replicates the asymptotic soil behavior in the test with a suction magnitude of 0 kPa. Moreover, the model effectively captures the influence of suction on soil compressibility when compared to the
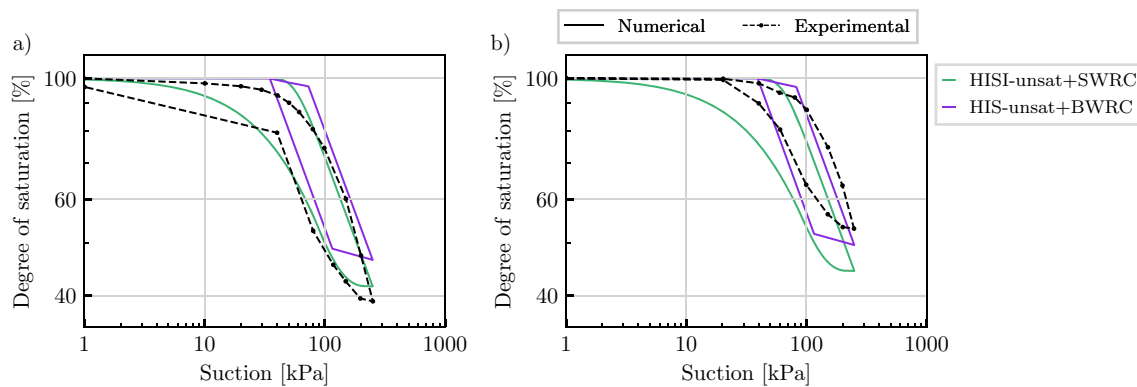
Fig. 2 Water retention behavior at two net confining pressures **a** $p^{net} = 110$ kPa **b** $p^{net} = 300$ kPa (experimental results by Ng et al. [28] and model simulations). dashed lines = experimental results, solid lines = numerical predictions

experimental tests for most of the considered suction values. The model successfully reproduces the increase in stiffness induced by suction, with the slope of the normal compression line decreasing as suction increases. However, it was noted that at the highest suction magnitude ($s = 200$ kPa), the slope is overestimated. Another limitation is associated with the experimental data trend observed in the test conducted at a suction value of 50 kPa. According to Ng and Yung [29], this deviation is attributed to the fact that this particular sample was the first prepared using moist tamping, leading to a higher initial void ratio compared to the other specimens. Consequently, the model is unable to replicate this specific experiment. Nevertheless, the predicted slope magnitude for this simulation aligns with the expected behavior of unsaturated soils, as it decreases in comparison to the normal compression line for the saturated specimen ($s = 0$ kPa).
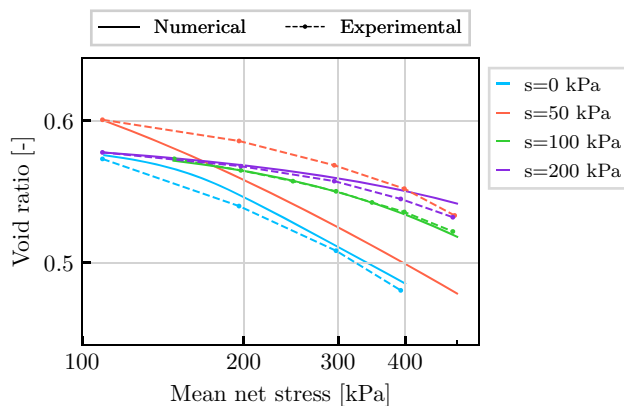
Fig. 3 Suction-controlled isotropic compression tests (experimental data by Ng and Yung [29] and numerical predictions). Dashed lines = experimental results, solid lines = numerical predictions using HISI-unsat+SWRC

4.3 Constant p^{net} triaxial tests under different hydraulic paths

Wong and Mašín [51] evaluated the "HIS-unsat+BWRC" model capabilities in the small strain range using triaxial tests under constant p^{net} conditions, following various wetting and drying paths. To demonstrate that the improvements made to the numerical model did not affect significantly the performance of the previous model, the following two sets of experiments conducted by Ng and Xu [27] were calibrated with the new model:

- The first set of experiments aimed to analyze the effect of suction magnitude on small strain stiffness. The tests began from a compacted state with a suction magnitude $s = 95$ kPa and a mean net stress of $p^{net} = 0$ kPa. Subsequently, the samples were loaded under isotropic conditions to a mean net stress of $p^{net} = 100$ kPa. In the subsequent stage, the samples were either dried to a suction value of $s = 150$ kPa or $s = 300$ kPa, or wet to a suction of $s = 1$ kPa. Finally, shearing under constant p^{net} conditions was applied to the samples and the stiffness degradation curve was recorded.
- The second set of experiments had the same initial state as the previous set. The initial stage was followed by applying drying and wetting stages to the samples, starting from a suction of 95 kPa and progressing to suctions of 300-150-50-150 kPa. Ultimately, the samples were sheared under two different mean net stresses: $p^{net} = 100$ and $p^{net} = 200$ kPa.

Additional information regarding the experimental program can be found in the study by Ng and Xu [27]. Figure 4a displays the results of the first set of experiments in comparison with numerical simulations conducted using "HISI-unsat+SWRC", presenting the shear modulus against the shear strain. For more details of the performance of "HIS-unsat+BWRC", readers are directed to Wong and Mašín [51]. The enhanced constitutive model

successfully reproduces the relationship depicted in the stiffness degradation curve concerning suction magnitude, wherein the shear modulus increases with the increase in suction. Furthermore, the model effectively captures the effects of suction on the deviatoric stress, as the predicted maximum deviatoric stress increases with higher suction levels, aligning with the experimental observations. See Fig. 4b.

In regard to the second set of experiments, the numerical model is able to predict different higher initial shear modulus G_{tp0} at elevated mean net stresses. The constitutive model also captures the stiffness degradation. Refer to Fig. 5a. for illustration. Moreover, the model effectively reproduces the trend in the deviatoric stress behavior, with the maximum deviatoric stress increasing proportionally with higher mean net stresses, as depicted in Fig. 5b.

At large strains, the response of the model under shearing is influenced by suction, as observed in Fig. 4b. There are two effects of suction accounted for by the model at large strains. Firstly, the soil strength increases due to suction, thanks to the factor χs in the definition of the effective stress equation (See Eq. 3), while the critical state friction angle is independent of suction. This effect can also be interpreted as an apparent cohesion due to suction. Additionally, the size of the State Boundary Surface (SBS) is defined to be dependent on suction. This effect can also be interpreted as an apparent over-consolidation due to suction, controlled by parameters n_s and l_s. These two parameters govern the distance between the normal compression line and the critical state line, as well as the peak strength.

4.4 Cyclic constant water content triaxial tests

In this section, the results of the numerical simulations on cyclic constant water content triaxial tests are presented. The laboratory tests were taken from Ng et al. [30, 54].

They were performed using compacted samples with an initial suction of $s = 95$ kPa. The experimental procedure was as follows: first, the samples were loaded under isotropic conditions to a mean net stress of $p^{net} = 30$ kPa. Thereafter, the target suction values $s = \{0, 30, 60\}$ kPa were reached on the samples. In the final stage, one-way cyclic deviatoric stress in haversine form was applied under constant water content conditions. The amplitude of the deviatoric stress was $q^{amp} = 70$ kPa. Based on the experimental program, the numerical simulations were performed reproducing the complete pre-shearing history, starting from the as-compacted state. For this purpose, the initial void ratio was set equal to the average value reported in the experiments ($e_{init} = 0.57$). Additionally, the intergranular strain was initialized under oedometric conditions to simulate the effects of one-dimensional compaction, given by $\delta_{11} = -R(S_r)$, with the other components set equal to 0, thus implying $\|\boldsymbol{\delta}\| = R(S_r)$. For each test, the first irregular cycle was ignored with the purpose of focusing mainly on reproducing the accumulated rate of strain, as the deformation from the first cycle significantly differs from the subsequent cycles [46, 49].

Initially, the numerical simulations were performed using the calibrated parameters by Wong and Mašín [51] and the original model formulation "HIS-unsat+BWRC". Despite this set of parameters accurately predicted the small strain behavior and asymptotic states of the material, as presented in Wong and Mašín [51] under monotonic loading, the same set of parameters failed to reproduce the cyclic behavior of the material, as observed in Fig. 6. The numerical simulations with this parameter set over-predicted the accumulated shear strain for all suction magnitudes, see Fig. 6a,b,c. Therefore, it became evident that a re-calibration was necessary. In addition, Fig. 6d shows that the accumulated strains are similar for the test at suction of 0 kPa and 30 kPa. This behavior could be explained as a result of the bi-linear formulation used for
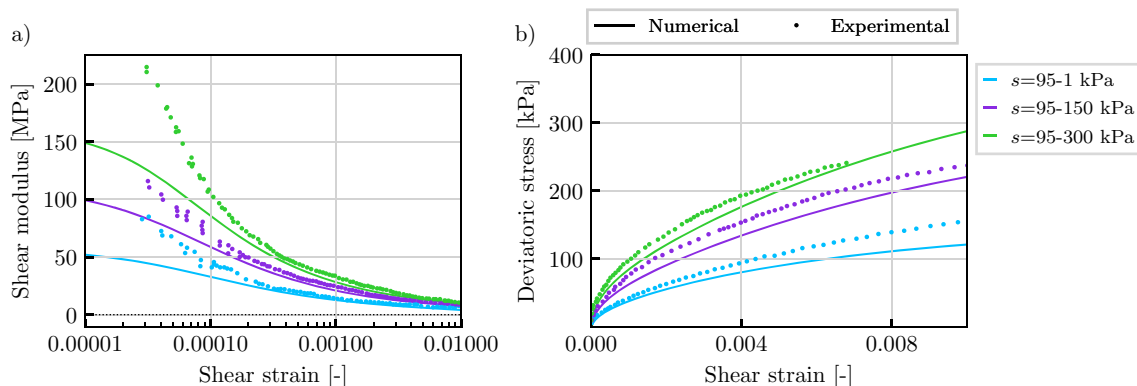

Fig. 4 First set of experiments under constant p^{net} triaxial conditions test **a** shear modulus versus shear strain; **b** deviatoric stress versus shear strain (experimental data by Zhou [54] and model predictions). Points = experimental results, solid lines = numerical predictions
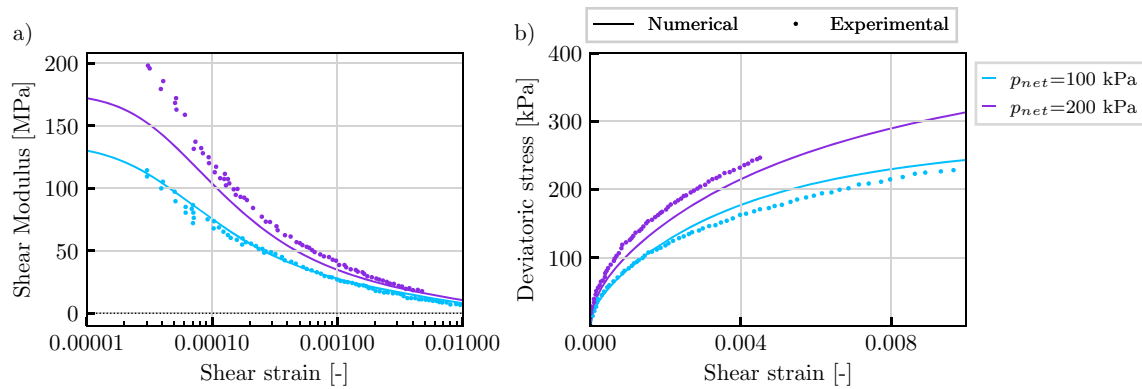
Fig. 5 Second set of experiments under constant p^{net} triaxial conditions test **a** shear modulus versus shear strain; **b** deviatoric stress versus shear strain (experimental data by Zhou [54] and model predictions). Points = experimental results, solid lines = numerical predictions

the water retention curve. This formulation causes both suction values to be in fully saturated state because the water retention curve does not distinguish between the drying and wetting branch for small suction magnitudes. Conversely, the smoothed formulation can capture the differences in the degree of saturation at a suctions of 0 kPa and 30 kPa during the wetting path. This difference in formulation influences the mechanical response due to the coupled characteristics of the model. This observation also explains the reason that prompted the authors to extend the previous "HIS-unsat+BWRC" formulation with the smoothed water retention curve, as proposed by Svoboda et al. [37]. Another remark is that this set of parameters failed to achieve convergence for more than 95 cycles at the suction magnitude of 60 kPa, as depicted in Fig. 6c and d.

Figure 7a, c, and e shows the numerical predictions using the "HIS-unsat+SWRC" model for the suction magnitudes of 0, 30, and 60 kPa, respectively, in terms of the deviatoric stress versus shear strain. This model successfully predicts the total shear strain at each suction magnitude. Additionally, the model captures the increase in stiffness with suction, as the accumulated shear strain decreases with increasing suction. The results were also analyzed in terms of the accumulated strain versus the number of cycles, as shown in Fig. 8. To calculate the accumulated strain, the values of strain at the beginning and the middle of each cycle were stored. This approach results in the colored area representing the accumulated strain in each cycle, while the border lines correspond to the value at the beginning and middle of each cycle, respectively.

As observed in Fig. 8, the "HIS-unsat+SWRC" fails to reproduce the rate of accumulated strain presented in the experimental results. In this model, the rate of accumulated strain increases linearly with the increment in the number of cycles, which differs from the experimental evidence

where the rate of accumulated strain decreases as the number of cycles increases. In contrast, the "HISI-un-sat+SWRC" model successfully captures the behavior of the soil at 0 suction magnitude, as it is able to predict both the accumulated shear strain and the rate of strain accumulation, see Figs. 7b and 8a. However, the magnitude of the strain is quantitatively under-predicted for the suction values of 30 kPa and over-predicted for the values of 60 kPa.

The secant shear modulus was also calculated for each cycle considering values of strain at maximum and minimum of the applied deviatoric stress as presented in Fig. 9. The predictions using "HIS-unsat+BWRC" under-predicted the secant shear modulus at each suction value. Meanwhile, using the "HIS-unsat+SWRC" model, the secant shear modulus is over-predicted at each suction value. This suggests that the strain accumulation in each cycle is smaller than the experimental observations, even though the total accumulation is fairly well predicted by this model. Consistently with the accurate predictions of the "HISI-unsat+SWRC" model for the accumulated rate of strain, the value of the secant shear modulus at each suction magnitude is well reproduced, along with its increasing tendency with increasing suction.

5 Summary and conclusions

In this study, the coupled hydro-mechanical model for partially saturated soils predicting small strain stiffness developed by Wong et al. [52] has been further extended to capture relevant features of unsaturated soil behavior under monotonic and cyclic loading. The enhancements include a smoothed formulation of the water retention curve, introduced by Svoboda et al. [37], which effectively captures the nonlinear dependency of the degree of saturation on suction. Furthermore, the intergranular strain concept has
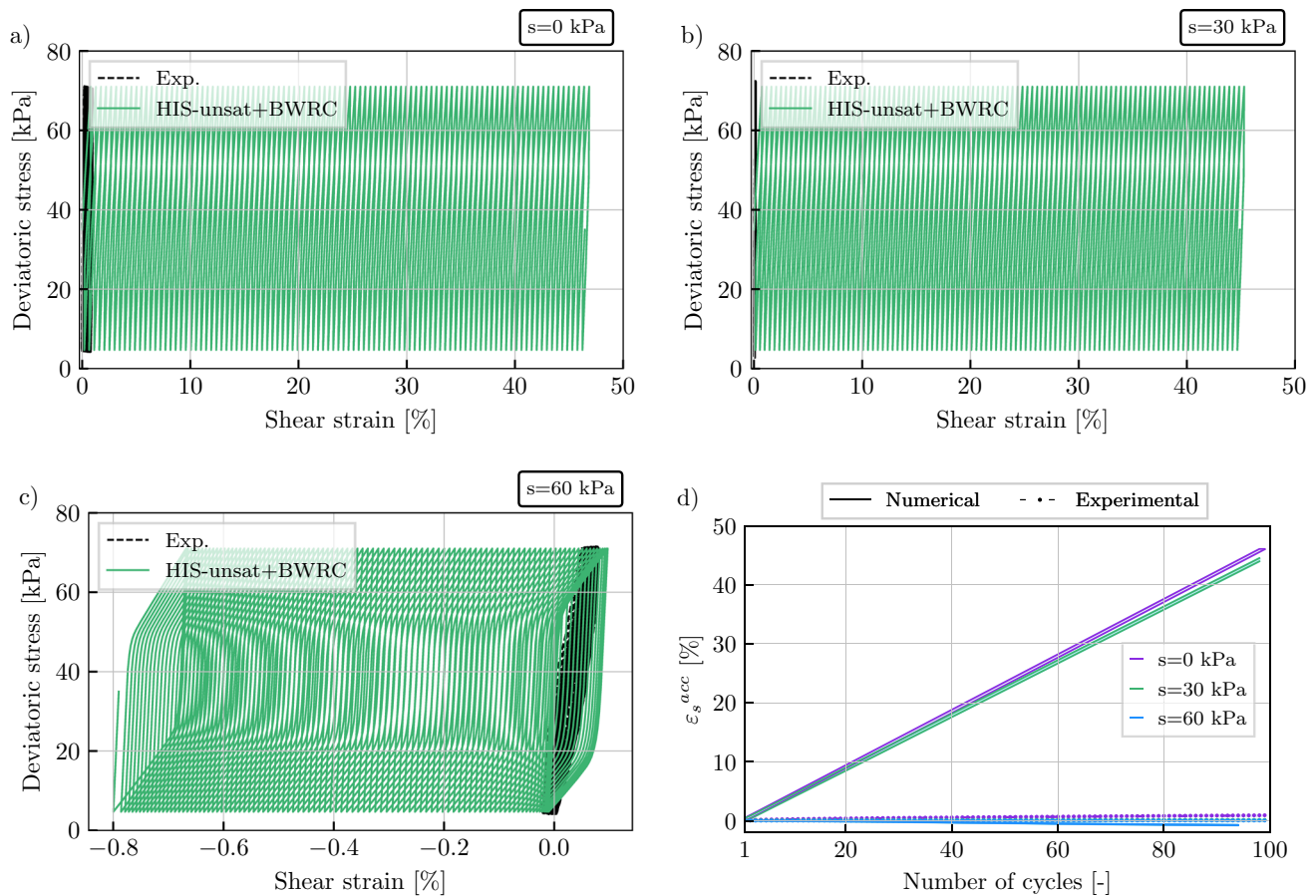
Fig. 6 Constant water cyclic triaxial test. Experimental results by Zhou [54] compared with numerical simulations using the reference model "HIS-unsat+BWRC" as calibrated by Wong and Mašín [51] for three suction magnitudes **a** $s = 0$ kPa **b** $s = 30$ kPa **c** $s = 60$ kPa **d** accumulated shear strain versus number of cycles

been replaced by the incorporation of the ISI concept, defined by Duque et al. [3], to model the relation between the strain accumulation rate and the number of cycles. Moreover, the ISI concept has been extended even further to encompass the influence of the degree of saturation.

The model's capabilities were assessed through the comparison of element test simulations employing both the enhanced model and the previous formulation against experimental data from the literature, using a completely decomposed tuff. The outcomes demonstrated that the revised model provides enhanced accuracy in capturing the effects of cyclic loading in partially saturated soils, exemplified by: (1) the improved water retention curve enables more realistic predictions of the soil's hydraulic response. This refinement also contributes to a more precise replication of the soil behavior under cyclic loading at various suctions magnitudes, due to the well-distinguished wetting and drying paths thanks to the hysteretical effects; (2) the incorporation of the ISI concept in the model's formulation, leads to better capturing of strain accumulation rates. Consequently, the strain accumulation rate

diminishes with increasing number of cycles; (3) additionally, the model qualitatively reproduces the relationship between strain accumulation and degree of saturation, displaying a reduction in the accumulated strain as the degree of saturation decreases.

Moreover, it was demonstrated that the previous model capabilities are not influenced by the changes added into the new model formulation. For that purpose, the numerical model was evaluated in monotonic loading under isotropic loading and shearing. The results showed that the numerical model is able to predict the effects of suction on soil response. The model predicts an increase in shear strength due to suction, while maintaining the critical state friction angle constant. Additionally, the size of the state boundary surface is defined to be dependent on suction, by introducing a dependency of the normal compression line on suction. Thus, the model predicts an apparent over-consolidated response when suction increases. Additionally, the model can also be used for reproduction of wetting-induced collapse.
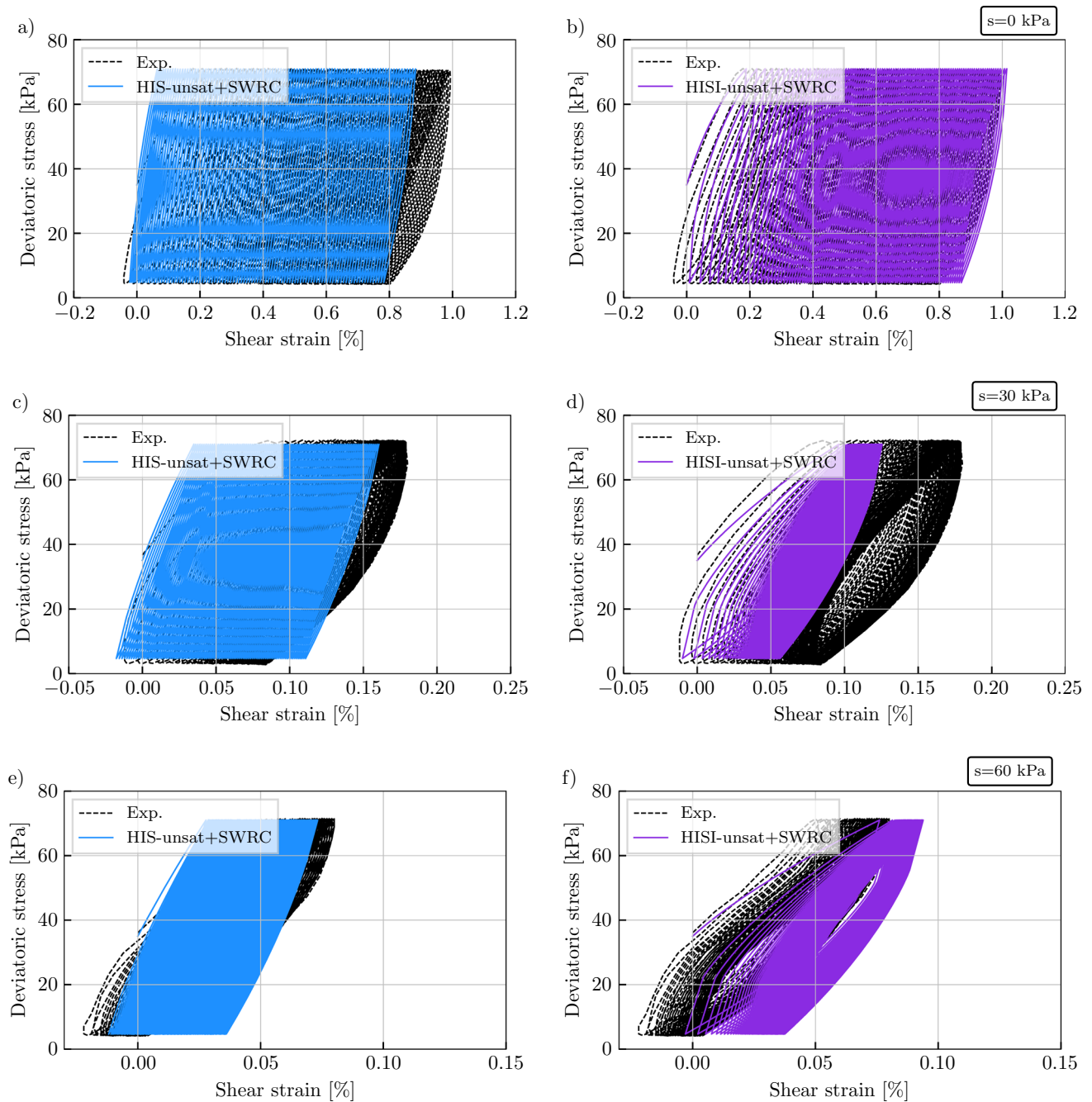
Fig. 7 Comparison of cyclic constant water triaxial tests as performed by Zhou [54] and numerical simulations performed using "HIS-unsat+SWRC" and "HISI-unsat+SWRC" at three suction levels **a,b** $s = 0$ kPa, **c,d** $s = 30$ kPa and **e,f** $s = 60$ kPa

Despite the congruent predictions of the enhanced constitutive model, certain limitations persist. Notably, the following points deserve to be remarked: firstly, concerning hydraulic behavior, the model fails to fully capture the dependency of the water retention curve on void ratio. Secondly, the model's predictions of strain accumulation rates at different suctions exhibit under-prediction for a suction of 30 kPa and over-prediction for a suction of 60 kPa. The ongoing efforts of the authors involve incorporating temperature effects into the model's response.

Appendix 1: notation

The notation and convention is as follows: scalar magnitudes (e.g., a, b) are denoted by italic fonts, second-order tensors (e.g., $\mathbf{A}$, $\mathbf{B}$) with bold capital letter or bold symbols,
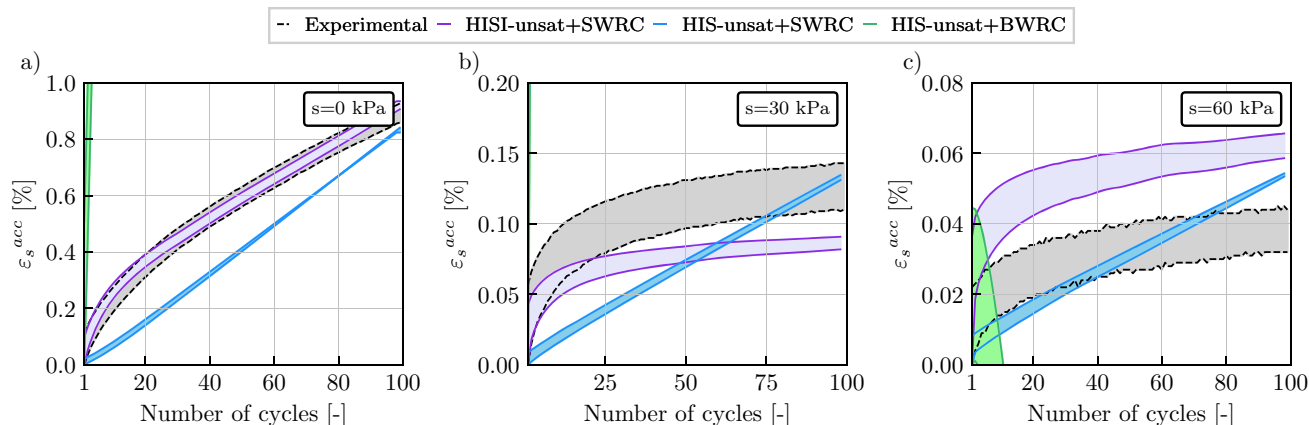
Fig. 8 Comparison of the accumulated shear strain versus number of cycles using the numerical models (HISI-unsat+SWRC, HIS-unsat+SWRC and HIS-unsat+BWRC) and the experimental data from cyclic constant water triaxial tests at three suction levels **a** $s = 0$ kPa, **b** $s = 30$ kPa and **c** $s = 60$ kPa
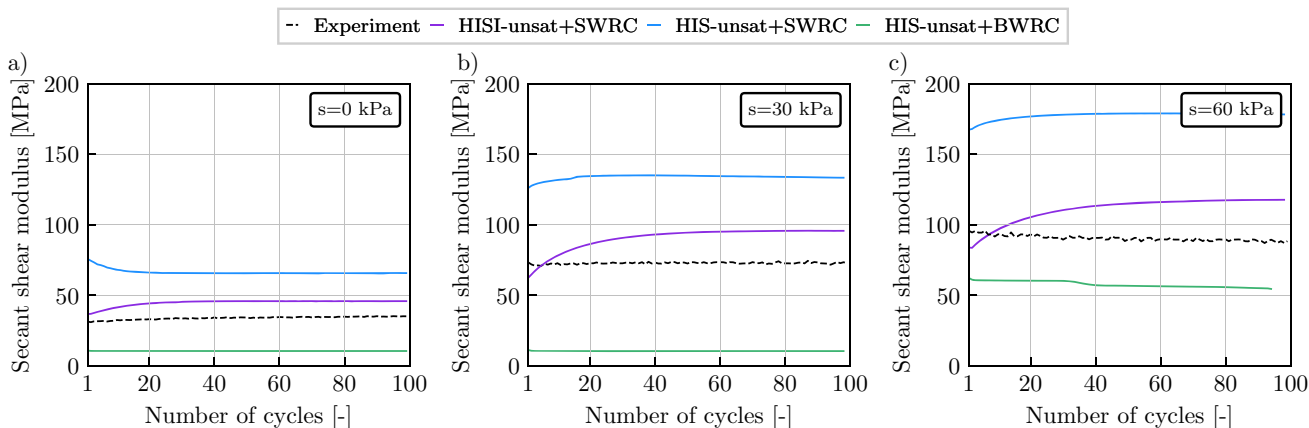

Fig. 9 Secant shear modulus versus number of cycles using the numerical models HISI-unsat+SWRC, HIS-unsat+SWRC and HIS-unsat+BWRC and the experimental data from cyclic constant water triaxial tests at three suction levels **a** $s = 0$ kPa; **b** $s = 30$ kPa and **c** $s = 60$ kPa

and fourth-order tensors with calligraphic bold letters (e.g., $\mathcal{L}, \mathcal{M}$). Components of these tensors are denoted through indicial notation (e.g., A_{ij}). δ_{ij} is the Kronecker delta, also represented with ($\boldsymbol{I}_{ij} = \delta_{ij}$). The unit fourth-rank tensor for symmetric tensors is denoted by $\mathcal{I}$, where $\mathcal{I}_{ijkl} = \frac{1}{2}\left(\delta_{ik}\delta_{jl} + \delta_{il}\delta_{jk}\right)$. The following operations hold: $\mathbf{A} : \mathbf{B} = A_{ij}B_{ij}$, $\mathbf{A} \otimes \mathbf{B} = A_{ij}B_{kl}$, $\| \mathbf{A} \| = \sqrt{A_{ij}A_{ij}}$, $\overrightarrow{\Box} = \frac{\Box}{\|\Box\|}$, $\mathbf{A}^{\text{dev}} = \mathbf{A} - \frac{1}{3}(\text{tr}\mathbf{A})\mathbf{1}$, $\hat{\mathbf{A}} = \frac{\mathbf{A}}{\text{tr}(\mathbf{A})}$. The product represented by '∘' is defined as $(\mathbf{p} \circ \mathbf{1})_{ijkl} = \frac{1}{2}(p_{ik}1_{jl} + p_{il}1_{jk} + p_{jl}1_{ik} + p_{jk}1_{il})$. The operator $\langle x \rangle$ represents the positive part of any scalar function x, therefore $\langle x \rangle = (x + |x|)/2$. Components of the effective stress tensor $\boldsymbol{\sigma}$ or strain tensor $\boldsymbol{\varepsilon}$ in compression are negative. Roscoe variables are defined as $p = -\sigma_{ii}/3$,

$q = \sqrt{\frac{3}{2}} \| \boldsymbol{\sigma}^{\text{dev}} \|$, $\varepsilon_v = -\varepsilon_{ii}$ and $\varepsilon_s = \sqrt{\frac{2}{3}} \| \boldsymbol{\varepsilon}^{\text{dev}} \|$. The stress ratio η is defined as $\eta = q/p$.

Appendix 2: complete mathematical description of the constitutive model

In this appendix, a summary of the constitutive relations of the hypoplastic model "HISI-unsat+SWRC" for fine-grained soils is provided. Table 8 includes the state variables evolution equations. Tables 7, 9 and 10 present all the constitutive relations that are part of the model formulation.

Table 8 State variables evolution equations

$$\dot{\boldsymbol{\sigma}}^{\text{net}} - \boldsymbol{I}(1 - \gamma r_{\lambda\text{scan}})\chi\dot{s} = \mathcal{M}^{HM} : \dot{\boldsymbol{\varepsilon}} + f_u\mathbf{H}_s \quad \text{For saturated conditions:}$$
$$\dot{\boldsymbol{\sigma}}^{\text{net}} - \boldsymbol{I}\dot{s} = \mathcal{M} : \dot{\boldsymbol{\varepsilon}}$$

$$\dot{a}_{\text{scan}} = \frac{1 - r_{\lambda\text{scan}}}{s_D(1 - a_e)}\dot{s}$$

$$\dot{s}_{\text{en}} = -\frac{\gamma s_{\text{en}}}{e\lambda_{psu}}\dot{e}$$

$$\dot{e} = (1 + e)\text{tr}\dot{\boldsymbol{\varepsilon}}$$

$$\dot{\boldsymbol{\delta}} = \begin{cases} \left(\mathcal{I} - \hat{\boldsymbol{\delta}} \otimes \hat{\boldsymbol{\delta}}\rho^{\beta_r}\right) : \dot{\boldsymbol{\varepsilon}} - \boldsymbol{\delta}\frac{\langle -\dot{R}(S_r)\rangle}{R(S_r)} & \text{for } \hat{\boldsymbol{\delta}} : \dot{\boldsymbol{\varepsilon}} > 0 \\ \dot{\boldsymbol{\varepsilon}} & \text{for } \hat{\boldsymbol{\delta}} : \dot{\boldsymbol{\varepsilon}} \leq 0 \end{cases}$$

$$\dot{R}(S_r) = r_m\left(-\frac{\dot{S}_r}{S_r\lambda_p} + \frac{\gamma}{e\lambda_{psu}}\dot{e}\right)$$

$$\dot{\Omega} = C_\Omega(1 - \rho^{\gamma_g} - \Omega)\|\dot{\boldsymbol{\varepsilon}}\|$$

Parameters φ_c, λ^*, κ^*, N, v_{pp}, α_G, n_s, l_s, m, $s_{\text{en}0}$, e_0, λ_{p0}, a_e, A_g, n_g, m_g, k_g, R, β_r, m_{rat}, r_m, $p_r = 1$ kPa, χ_{g0}, χ_{max}, C_Ω, γ_{chi}, ϑ_w.

State variables $\boldsymbol{\sigma}^{\text{net}}$, s, S_r, e, a_{scan}, $\boldsymbol{\delta}$, s_{en}, Ω.

Appendix 3: description of model parameters, calibration procedure and state variables initialization

In this section, the model parameters along with their calibration procedure are thoroughly explained. For simplicity, the model parameters can be divided into five different groups regarding the features they are related to, as follows:

- *Basic hypoplasticity parameters* (φ_c, λ^*, κ^*, N, v_{pp}, α_G): The parameters in this group control the compressibility and shearing behavior of the soil under large strains.

They were introduced by Mašín [18]. φ_c corresponds to the critical state friction angle, v controls the model response under shearing, it has the meaning of the Poisson's ratio, however its effect is different compared to elasto-plastic models. An increase in v, decreases the predicted shear modulus. Additionally, it affects the evolution of excess pore water pressures in undrained conditions. Both parameters can be calibrated based on drained or undrained triaxial tests. The parameters λ^*, κ^* correspond to the slope of the normal compression line (NCL) and the slope of the loading/reloading line, respectively. Meanwhile, N controls the position of the normal compression line. For their calibration, isotropic/oedometric compression tests are needed. The parameter α_G was introduced in the hypoplastic model with very small strain stiffness anisotropy [19] and it corresponds to the ratio between the shear moduli within the plane of isotropy G_{pp} and the transversal plane of isotropy G_{tp}. For its calibration, wave propagation measurements are needed. Some authors have suggested approximations of this parameter when this type of data is not available (See [24]). A value of $\alpha_G = 1$ is associated to isotropic materials. For more details, the reader is referred to [8].

- *Unsaturated mechanical effects* (n_s, l_s, m): The unsaturated mechanical response of the constitutive model is controlled by this group of parameters. n_s influences the position of the unsaturated normal compression lines with respect to the saturated normal compression line. Additionally, l_s is introduced to model the change in the slope of the normal compression line with suction. For calibrating these two parameters isotropic/oedometric compression test under different saturation conditions are needed. The parameter m influences wetting-

Table 9 Constitutive relations related to the hydraulic water retention behavior

$$S_r = \left(\frac{s_e}{s}\right)^{\lambda_p} \qquad\qquad \text{For saturated conditions: } S_r = 1.0$$

$$\lambda_{psu} = \frac{\gamma}{\ln\chi_{0su}}\ln\left[\left(\chi_{0su}^{(\lambda_{p0}/\gamma)} - \chi_{0su}\right)\left(\frac{e}{e_0}\right)^{(\gamma-1)} + \chi_{0su}\right] \qquad\qquad \chi_{0su} = \left(\frac{s_{\text{en}0}}{s_{\text{en}}}\right)^{\gamma}$$

$$\lambda_p = \frac{\gamma}{\ln\chi_0}\ln\left[\left(\chi_0^{\frac{\lambda_{p0}}{\gamma}} - \chi_0\right)\left(\frac{e}{e_0}\right)^{(\gamma-1)} + \chi_0\right] \qquad\qquad \chi_0 = \left(\frac{s_{\text{en}0}}{s}\right)^{\gamma}$$

$$s_e = s_{\text{en}}(a_e + a_{\text{scan}} - a_e a_{\text{scan}}) \qquad\qquad s_D = \frac{s_{\text{en}}}{s_e}s$$

$$f_{\text{scan}} = \begin{cases} a_{\text{scan}} & \text{for } \dot{s} > 0 \\ 1 - a_{\text{scan}} & \text{for } \dot{s} < 0 \end{cases} \qquad\qquad a_{\text{scan}} = \frac{s - s_W}{s_D - s_W}$$

$$r_\lambda = \begin{cases} 0 & \text{for } s < a_e s_{\text{en}} \text{ and } \dot{s} > 0 \\ \left(\frac{1 - S_r}{1 - S_{\lim}}\right)^{p_{\text{wett}}} & \text{for } S_r > S_{\lim} \text{ and } \dot{s} < 0 \\ f_{\text{scan}}^{p_{\text{scan}}} & \text{otherwise} \end{cases} \qquad\qquad \gamma = 0.55 \text{ [12]}$$

$$r_{\lambda\text{scan}} = \begin{cases} 0 & \text{for } s < a_e s_{\text{en}} \text{ and } \dot{s} > 0 \\ f_{\text{scan}}^{p_{\text{scan}}} & \text{otherwise} \end{cases}$$

Table 10 Constitutive relations of the hypoplastic model

$\boldsymbol{\sigma} = \boldsymbol{\sigma}^{\text{net}} - \boldsymbol{1}\chi s$

$\chi = \left(\frac{s_e}{s}\right)^{\gamma}$

$\boldsymbol{\sigma}^{\text{net}} = \boldsymbol{\sigma}^{tot} + u_a$

$s = u_a - u_w$

$\hat{\boldsymbol{\delta}} = \begin{cases} \dfrac{\boldsymbol{\delta}}{\|\boldsymbol{\delta}\|} & \text{for } \boldsymbol{\delta} \neq \boldsymbol{0} \\ \boldsymbol{0} & \text{for } \boldsymbol{\delta} = \boldsymbol{0} \end{cases}$

$\rho = \dfrac{\|\boldsymbol{\delta}\|}{R(S_r)}$

$R(S_r) = R - \dfrac{r_m}{\lambda_p}\ln S_r$

$\hat{\boldsymbol{\sigma}}^{\text{dev}} = \dfrac{\boldsymbol{\sigma}}{\text{tr}\boldsymbol{\sigma}} - \dfrac{\boldsymbol{1}}{3}$

$\mathcal{M} = [\rho^{\chi_g}m_T + (1 - \rho^{\chi_g})m_R]f_s\mathcal{L}$

$+ \begin{cases} \rho^{\chi_g}(1 - m_T)f_s\mathcal{L} : \hat{\boldsymbol{\delta}} \otimes \hat{\boldsymbol{\delta}} + \rho^{\gamma_g}f_sf_d\mathbf{N}\hat{\boldsymbol{\delta}} & \text{for } \hat{\boldsymbol{\delta}} : \dot{\boldsymbol{\varepsilon}} > 0 \\ \rho^{\chi_g}(m_R - m_T)f_s\mathcal{L} : \hat{\boldsymbol{\delta}} \otimes \hat{\boldsymbol{\delta}} & \text{for } \hat{\boldsymbol{\delta}} : \dot{\boldsymbol{\varepsilon}} \leq 0 \end{cases}$

$\mathcal{M}^{HM} = \mathcal{M} - \dfrac{s(1 + e)\gamma^2}{e\lambda_{psu}}\left(\dfrac{s_{en}}{s}\right)^{\gamma}\boldsymbol{1} \otimes \boldsymbol{1}$

$\chi_g = \chi_{g0} + \Omega(\chi_{\max}(S_r) - \chi_{g0})$

$\gamma_g = \gamma_\chi\chi_g$

$\chi_{\max}(S_r) = \chi_{\max}S_r^{\vartheta_w}$

$\mathcal{L} = \dfrac{1}{2}a_1\boldsymbol{1} \circ \boldsymbol{1} + a_2\boldsymbol{1} \otimes \boldsymbol{1} + a_3(\mathbf{p} \otimes \boldsymbol{1} + \boldsymbol{1} \otimes \mathbf{p}) + a_4\mathbf{p} \circ \boldsymbol{1} + a_5\mathbf{p} \otimes \mathbf{p}$

$p_{ij} = n_i n_j^{\dagger}$

$a_1 = \alpha_E\left(1 - v_{pp} - 2\dfrac{\alpha_E}{\alpha_v^2}v_{pp}^2\right)$

$a_2 = \alpha_E v_{pp}\left(1 + \dfrac{\alpha_E}{\alpha_v^2}v_{pp}\right)$

$a_3 = \alpha_E v_{pp}\left(\dfrac{1}{\alpha_v} + \dfrac{v_{pp}}{\alpha_v} - 1 - \dfrac{\alpha_E}{\alpha_v^2}v_{pp}\right)$

$a_4 = \alpha_E\left(1 - v_{pp} - 2\dfrac{\alpha_E}{\alpha_v^2}v_{pp}^2\right)\dfrac{1 - \alpha_G}{\alpha_G}$

$a_5 = \alpha_E\left(1 - \dfrac{\alpha_E}{\alpha_v^2}v_{pp}^2\right) + 1 - v_{pp}^2 - 2\dfrac{\alpha_E}{\alpha_v}v_{pp}(1 + v_{pp}) - \dfrac{2\alpha_E}{\alpha_G}\left(1 - v_{pp} - 2\dfrac{\alpha_E}{\alpha_v^2}\alpha_{pp}^2\right)$

$\alpha_E = \alpha_G^{(1/x_{GE})}$

$\alpha_v = \alpha_G^{(1/x_{Gv})}$

$x_{GE} = 0.8$

$x_{Gv} = 1$

$\mathbf{N} = -\dfrac{\mathcal{A} : \mathbf{d}}{f_s f_d^A}$

$\mathbf{d} = \dfrac{\mathbf{d}^A}{\|\mathbf{d}^A\|}$

$\mathbf{d}^A = -\hat{\boldsymbol{\sigma}}^{\text{dev}} + \boldsymbol{1}\left[\dfrac{2}{3} - \dfrac{\cos 3\theta + 1}{4}F_m^{1/4}\right]\dfrac{F_m^{\xi/2} - \sin^{\xi}\varphi_c}{1 - \sin^{\xi}\varphi_c}$

$\xi = 1.7 + 3.9\sin^2\varphi_c$

$\cos(3\theta) = -\sqrt{6}\dfrac{\text{tr}(\hat{\boldsymbol{\sigma}}^{\text{dev}}\hat{\boldsymbol{\sigma}}^{\text{dev}}\hat{\boldsymbol{\sigma}}^{\text{dev}})}{[\hat{\boldsymbol{\sigma}}^{\text{dev}} : \hat{\boldsymbol{\sigma}}^{\text{dev}}]^{3/2}}$

$\tan\psi = \sqrt{3}\|\hat{\boldsymbol{\sigma}}^{\text{dev}}\|$

$\mathcal{A} = f_s\mathcal{L} + \dfrac{\boldsymbol{\sigma}}{\lambda_{act}^*} \otimes \boldsymbol{1}$

$f_s = -\dfrac{3\text{tr}\boldsymbol{\sigma}}{2A_m}\left(\dfrac{1}{\lambda_{act}^*} + \dfrac{1}{\kappa^*}\right)$

$f_d = \left(\dfrac{2p}{p_e}\right)^{\alpha_f}$

$p_e = p_r\exp\left[\dfrac{N(s) - \ln(1 + e)}{\lambda^*(s)}\right]$

$f_d^A = 2^{\alpha_f}(1 - F_m)^{\alpha_f/\omega}$

$F_m = \dfrac{9I_3 + I_1I_2}{I_3 + I_1I_2}$

$\omega = -\dfrac{\ln(\cos^2\varphi_c)}{\ln 2} + a(F_m - \sin^2\varphi_c)$

$a = 0.3$

$I_1 = \text{tr}\boldsymbol{\sigma}, I_2 = \dfrac{1}{2}\left[\boldsymbol{\sigma} : \boldsymbol{\sigma} - (I_1)^2\right]$

$I_3 = \det\boldsymbol{\sigma}$

$\alpha_f = \dfrac{\ln\left[\dfrac{\lambda^* - \kappa^*}{\lambda^* + \kappa^*}\left(\dfrac{3 + a_f^2}{a_f\sqrt{3}}\right)\right]}{\ln 2}$

$a_f = \dfrac{\sqrt{3}(3 - \sin(\varphi_c))}{2\sqrt{2}\sin(\varphi_c)}$

$\mathbf{H}_s = -\dfrac{c_i r_{\lambda\text{scan}}\boldsymbol{\sigma}}{s\lambda^*(s)}\left(n_s - l_s\ln\dfrac{p_e}{p_r}\right)\langle -\dot{s}\rangle$

$c_i = \dfrac{(\lambda_{act}^* + \kappa^*)(2^{\alpha_f} - f_d) + 2\kappa^*f_d}{(\lambda_{act}^* + \kappa^*)(2^{\alpha_f} - f_d^A) + 2\kappa^*f_d^A}$

$f_u = \left(\dfrac{f_d}{f_d^A}\right)^{(m/\alpha_f)}$

$\lambda_{act}^* = \lambda^*(s)\dfrac{e\lambda_{psu}}{e\lambda_{psu} - \gamma(1 + e)[n_s - l_s ln(p/p_r)]}$

$N(s) = N + n_s\left\langle\ln\left(\dfrac{s}{s_e}\right)\right\rangle$

$\lambda^*(s) = \lambda^* + l_s\left\langle\ln\left(\dfrac{s}{s_e}\right)\right\rangle$

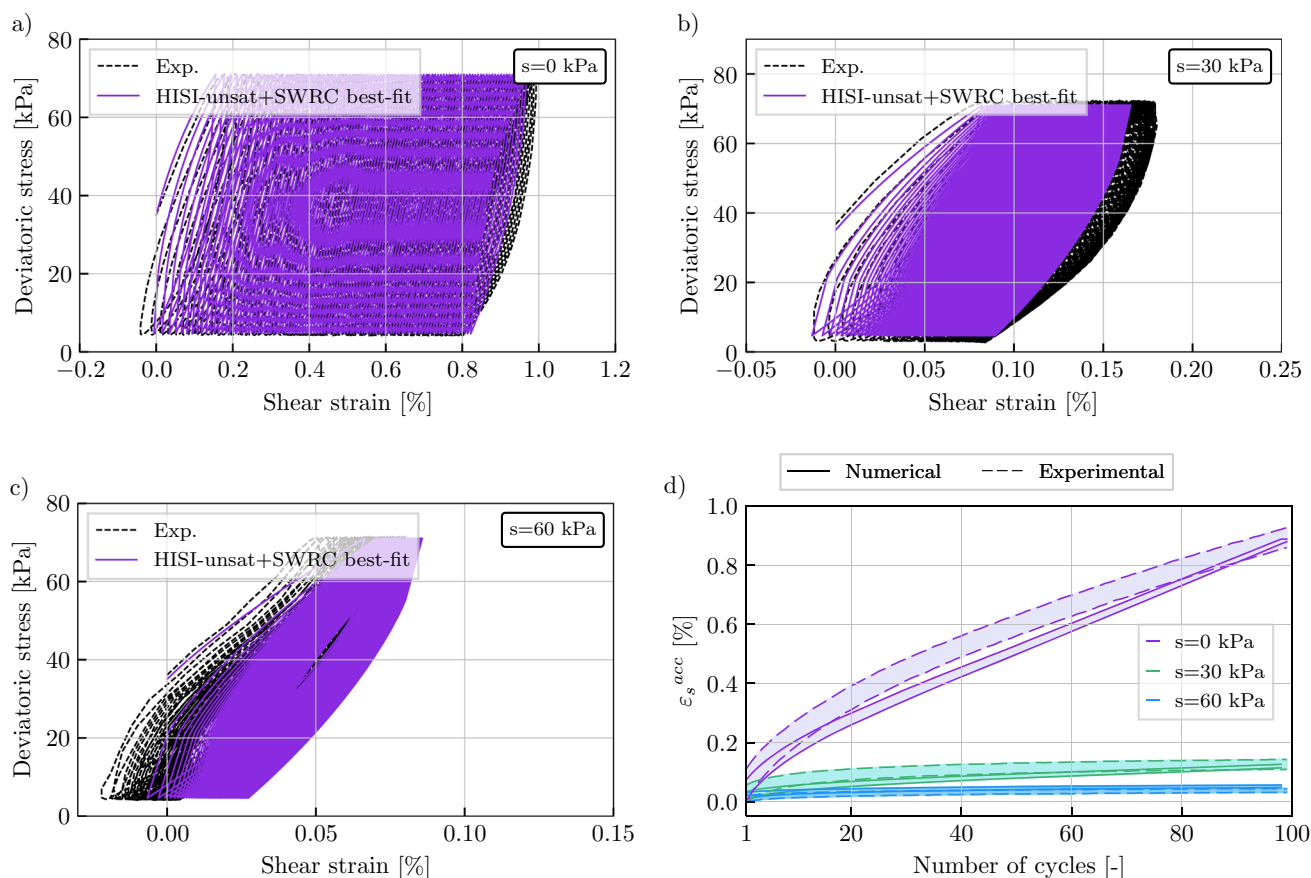† n_i is a unit vector normal to the plane of symmetry in transversely isotropic material

Fig. 10 Constant water cyclic triaxial. Experimental results by Zhou [54] compared with numerical simulations using "HISI-unsat+SWRC" calibrated for the best fit of the new parameter ϑ_w for three suction magnitudes **a** $s = 0$ kPa, **b** $s = 30$ kPa, **c** $s = 60$ kPa, **d** accumulated shear strain versus number of cycles

induced collapse and it describes the rate at which the soil becomes less susceptible to collapse as the distance from the SBS increases. It can be calibrated based of a parametric study using wetting test on slightly over-consolidated soil. More information related to the parameters controlling unsaturated mechanical effects can be found in [22] and [23].

- *Water retention behavior* ($s_{en0}, e_0, \lambda_{p0}, a_e$): The hydraulic response of the model is controlled by the smoothed water retention curve proposed by Svoboda et al.[37]. For calibrating this group of parameters measurements

of the water retention curve of the soil should be employed. The values of e_0 and s_{en0} correspond to a reference void ratio and a reference air entry value of suction, at which the measurement of the WRC has been performed. λ_{p0} represents the slope of the main drying/wetting curve and a_e is a parameter controlling the ratio between the main drying and wetting curve.

- *Very small strain stiffness effects* (A_g, n_g, m_g, k_g): This group of parameters control the shear modulus at very small strains. The calibration of this set of parameters requires shear wave measurements under very small strains at different confining pressures for parameter m_g and n_g and different degrees of saturation for calibrating parameter k_g.

- *Improved intergranular strain (ISI)* (R, β_r, χ_{g0}, χ_{max}, C_Ω, γ_χ, m_{rat}, r_m, ϑ_w, m_{rat}): The parameters in this group govern the response of the model under small strains. The parameter R represents the size of the elastic range in the intergranular space, β_r controls the stiffness degradation of the model. These two parameters can be calibrated with shear modulus degradation curves. In addition, the parameter r_m influences the size of the

Table 11 Value of the parameters that were studied for the sensitivity analysis

Parameter	-20%	Optimized value	$+20\%$
R	0.00016	0.0002	0.00024
β_r	0.048	0.060	0.072
χ_{g0}	0.12	0.15	0.18
χ_{max}	0.248	0.31	0.372

elastic range with the increment in suction. Thus, its calibration can be performed based on degradation curves measured under unsaturated conditions. Parameters χ_{g0} and $\chi_{\max}$ control the accumulation of strains or pore water pressure under cyclic mechanical tests at a small and large number of cycles, respectively. For that reason, the calibration of χ_{g0} should be performed by simulating the results of cyclic triaxial tests at a small number of cycles e.g.$(N < 10)$. Meanwhile, $\chi_{\max}$ will control the accumulation at a larger number of cycles. An important recommendation is evaluating the calibration in terms of the accumulated strains/pore-pressures in respect to the number of cycles for a better calibration. The parameter C_Ω governs the velocity at which the strain accumulation rate changes from $\chi = \chi_{g0}$ to $\chi = \chi_{\max}$. Its value can be determined based on the observed behavior of accumulated strains or accumulated pore water pressure of cyclic triaxial tests. γ_χ controls accumulated pore pressures under undrained conditions or accumulated strains during drained conditions. Its calibration is performed by simulating cyclic triaxial tests. More information regarding the parameters of the ISI model are given in [3]. Special attention is given to parameter ϑ_w in Appendix 5 as it has been newly added in this work.

Additionally, special attention should be given to the initialization of the state variables. A short-guide for its initialization is given according to the following:

- e_{init}: the initial void ratio can be initialized according to the reported initial values of the experimental test or according to the compression law of the constitutive model given in Eq. 12.
- S_r: the initialization of the degree of saturation is performed using Eq. 16.
- a_{scan}: The initial value of a_{scan} will depend on the suction history the user would like to simulate. For previous drying history, the state variable should be initialize $a_{scan} = 1$, meanwhile, for wetting history, its initial value is $a_{scan} = 0$.
- s_{en}: The initial value of s_{en} is calculated by numerical integration of Eq. 24 from e_0 to the initial void ratio e_{init}.
- $\boldsymbol{\delta}$: The intergranular strain tensor should be initialized according to the soil history the user would want to reproduce in the numerical simulations. For isotropic initialization, $\delta_{11} = \delta_{22} = \delta_{33} = -R(S_r)/\sqrt{3}$, meanwhile for oedometric conditions $\delta_{11} = -R(S_r)$ and the other components are initialized to 0, giving $\|\boldsymbol{\delta}\| = R(S_r)$. More details can be found in [31].
- Ω: This variable controls the transition between monotonic and cyclic loading in the ISI concept. The variable

is initialized equal to zero and it will evolve according to Eq. 35 for storing the information about the previously performed loading.

Appendix 4: determination of parameter ϑ_w

The parameter ϑ_w is introduced in this model for controlling the dependency of the strain rate of accumulation on the degree of saturation as outlined in Eq. (37). To establish this dependency, the constant water content cyclic triaxial tests performed by Ng and Zhou [30] were simulated and the parameter $\chi_{\max}$ was calibrated for each suction value as presented in Fig. 10. Subsequently, a regression was performed using the three optimized values of $\chi_{\max}$ at each degree of saturation, yielding Eq. (37). In this regard, ϑ_w can be calibrated by examining the outcomes of cyclic triaxial tests conducted under either constant water content or suction-controlled conditions, at various suction magnitudes, within the stress versus strain plane.

Appendix 5: sensitivity analysis

This section focuses on selecting certain parameters from the proposed model "HISI-unsat+SWRC" that are associated with ISI, for the purpose of studying their impact on the model's response. To achieve this, simulations were conducted under saturated conditions ($s = 0$ kPa), with multiple repetitions involving variations of each parameter by ± 20 %, while keeping the remaining parameters equal to the calibrated values outlined in Table 6. The parameters selected for the sensitivity analysis correspond to: R, β_r, χ_{g0}, $\chi_{\max}$, whose meaning was presented in Table 1. A brief summary of the varied values in each simulation presented within this section is provided in Table 11.

Figure 11 depicts the impact of the studied parameters in terms of the deviatoric stress versus the shear strain. As it is observed in Fig. 11a and b, higher values of the parameter R reduces the accumulation of strains. This effect arises because an elevated value of R increases the soil's elastic range. This trend is further evident in Fig. 12a, where diminishing the magnitude of R leads to a higher rate of accumulated strain. Importantly, it should be noted that this parameter exerts significant influence on the soil response; even a mere 20% variation causes the accumulated strain to escalate from 0.9 to 2.5%.

Variations of the parameter β_r yield an effect opposite to that of R: as β_r increases, the soil's stiffness decreases, leading to increased strain accumulation (refer to Fig. 11c, d). Conversely, lower β_r values result in less accumulation
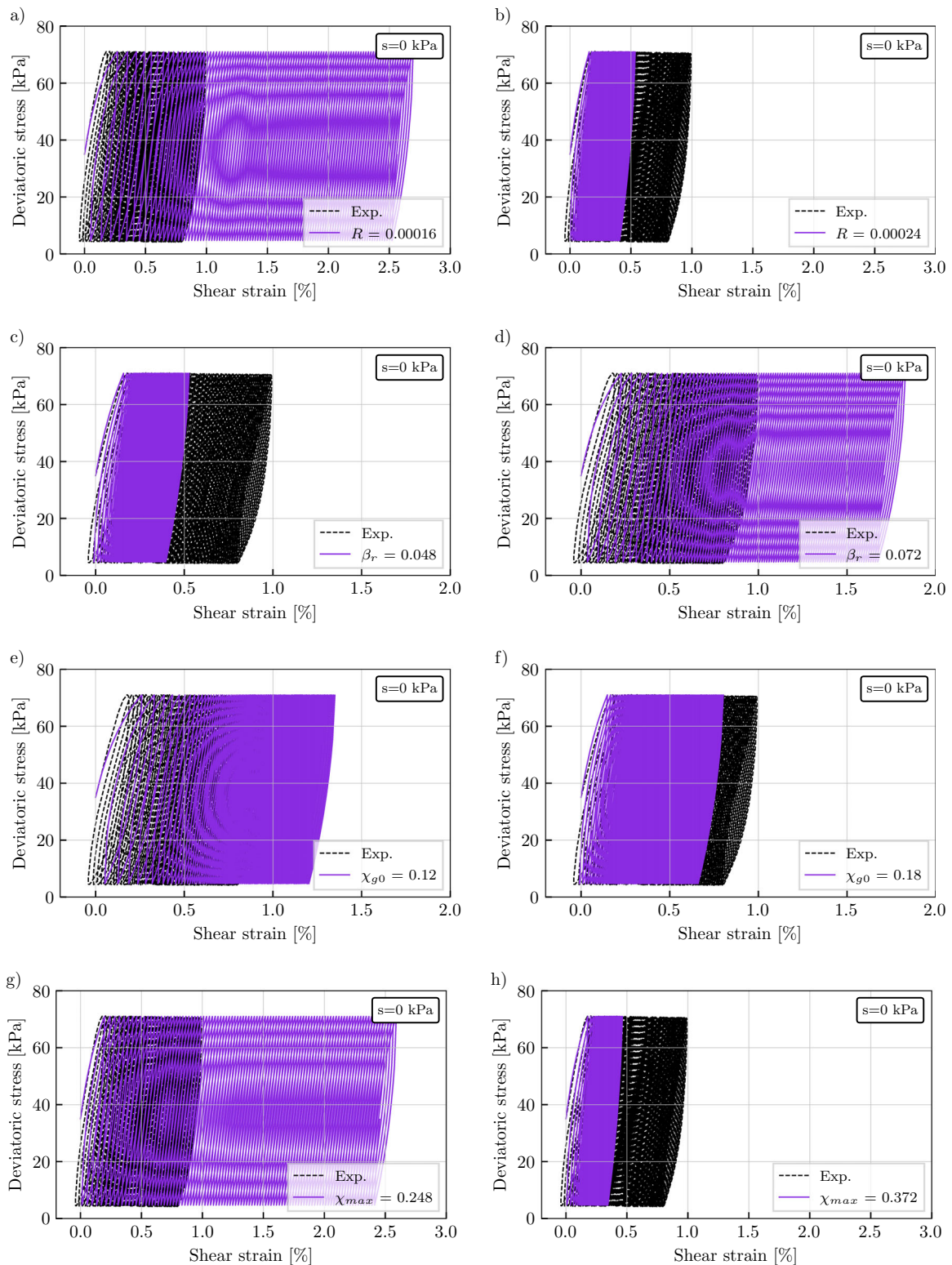
Fig. 11 Influence of the parameters related to small strain effects with $\pm$ 20% variation from the calibrated value **a** $R = 0.00016$, **b** $R = 0.00024$, **c** $\beta_r = 0.048$, **d** $\beta_r = 0.072$, **e** $\chi_{g0} = 0.12$, **f** $\chi_{g0} = 0.18$, **g** $\chi_{max} = 0.248$, **h** $\chi_{max} = 0.372$
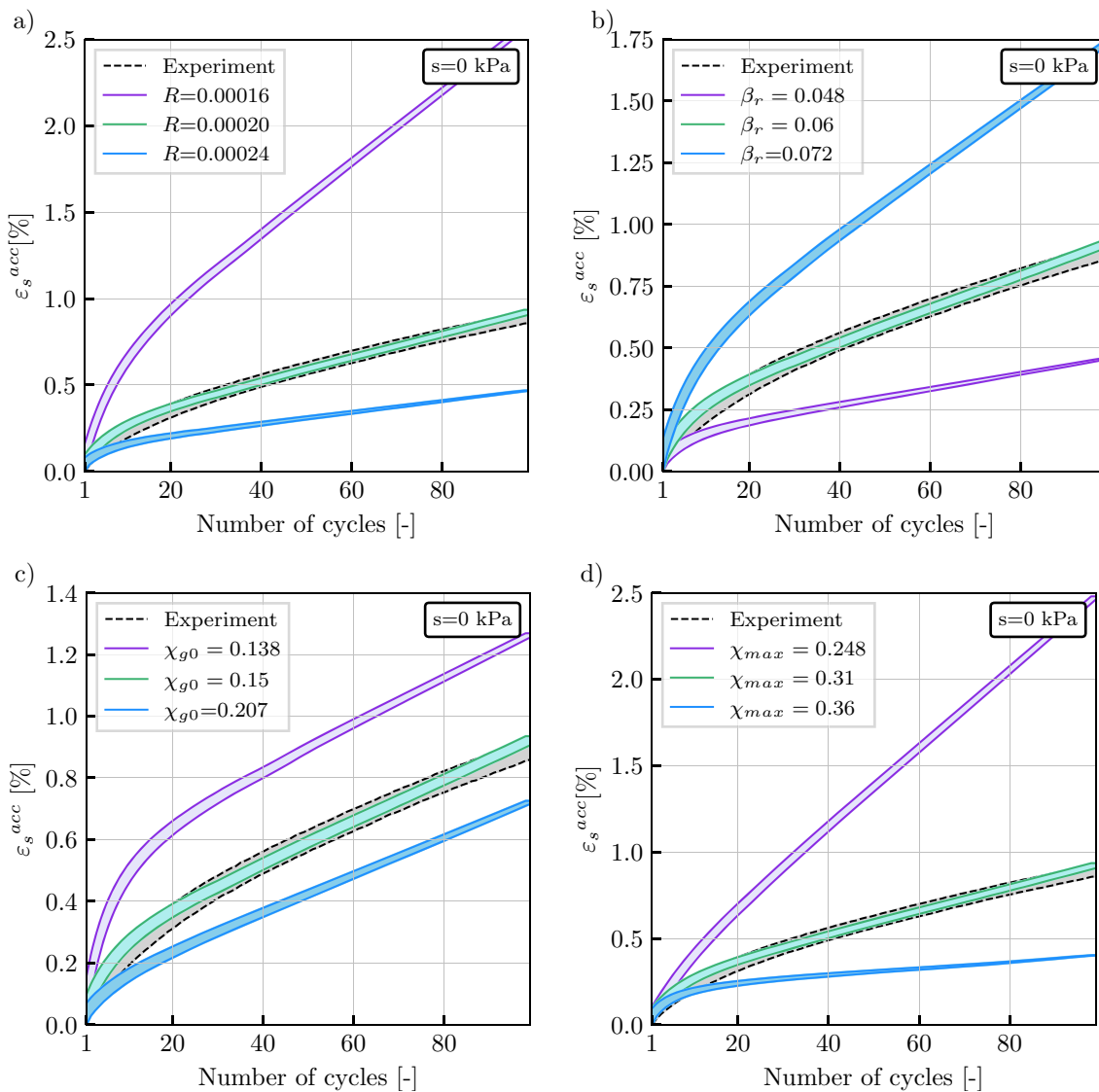
Fig. 12 Influence of the parameters related to small strain effects with ± 20% variation from the calibrated value in terms of ε_s^{acc} versus number of cycles **a** influence of parameter R, **b** influence of parameter β_r, **c** influence of parameter χ_{g0}, **d** influence of parameter χ_{max}

of strains, attributed to increased stiffness at higher β_r values. Figure 12b illustrates the analysis of accumulated shear strains in relation to the number of cycles. Notably, as observed, the influence of this parameter is comparatively less pronounced than that of R.

The impact of the parameters χ_{g0} and χ_{max} has also been subjected to analysis. As illustrated in Fig. 11e and f, reducing the value of χ_{g0} increases the strain accumulation, similar to decreasing the value of χ_{max} (refer to Fig. 11g and h). The distinction between these two parameters lies in their effect: χ_{g0} influences accumulation over a smaller number of cycles (e.g., $N < 10$), whereas χ_{max} manages the accumulation over a higher number of cycles (e.g., $N > 10$). This influence becomes clearer in Fig. 12c and d.

As observed, simulations with varied χ_{g0} exhibit diverse behavior during the initial cycles; subsequently, they show a parallel response after surpassing certain number of cycles. Conversely, simulations with different χ_{max} demonstrate the same response under smaller number of cycles performed, while the rate of accumulated shear strain changes after reaching a larger number of cycles.

Declarations

Conflict of interest The authors declare that they have no known competing financial interests or personal relationships that could have appeared to influence the work reported in this paper.

References

1. Boulanger RW, Price AB, Ziotopoulou K (2018) Constitutive modeling of the cyclic loading response of low plasticity fine-grained soils. In: Proceedings of GeoShanghai 2018 international conference: fundamentals of soil behaviours. Springer, pp 1–13
2. Brooks RH, Corey AT (1966) Properties of porous media affecting fluid flow. J Irrig Drain Div 92(2):61–88
3. Duque J, Mašín D, Fuentes W (2020) Improvement to the intergranular strain model for larger numbers of repetitive cycles. Acta Geotech 15:3593–3604
4. Duque J, Roháč J, Mašín D, Najser J (2022) Experimental investigation on Malaysian kaolin under monotonic and cyclic loading: inspection of undrained Miner's rule and drained cyclic preloading. Acta Geotech 17:4953–4975
5. Duque J, Roháč J, Mašín D, Najser J, Opršal J (2023) The influence of cyclic preloadings on cyclic response of Zbraslav sand. Soil Dyn Earthq Eng 166:107720
6. Duque J, Tafili M, Mašín D (2023) On the influence of cyclic preloadings on the liquefaction resistance of sands: a numerical study. Soil Dyn Earthq Eng 172:108025
7. Duque J, Tafili M, Seidalinov G, Mašín D, Fuentes W (2022) Inspection of four advanced constitutive models for fine-grained soils under monotonic and cyclic loading. Acta Geotech 17(10):4395–4418
8. Fuentes W, Mašín D, Duque J (2021) Constitutive model for monotonic and cyclic loading on anisotropic clays. Géotechnique 71(8):657–673
9. Fuentes W, Triantafyllidis T (2015) ISA model: a constitutive model for soils with yield surface in the intergranular strain space. Int J Numer Anal Methods Geomech 39(11):1235–1254
10. Janda T, Mašín D (2017) General method for simulating laboratory tests with constitutive models for geomechanics. Int J Numer Anal Methods Geomech 41(2):304–312
11. Jerman J, Mašín D (2020) Hypoplastic and viscohypoplastic models for soft clays with strength anisotropy. Int J Numer Anal Methods Geomech 44(10):1396–1416
12. Khalili N, Khabbaz M (1996) The concept of effective stress in unsaturated soils. University of New South Wales, School of Civil Engineering, Sydney
13. Kolditz O, Bauer S, Bilke L, Böttcher N, Delfs J-O, Fischer T, Görke UJ, Kalbacher T, Kosakowski G, McDermott C et al (2012) Opengeosys: an open-source initiative for numerical simulation of thermo-hydro-mechanical/chemical (thm/c) processes in porous media. Environ Earth Sci 67:589–599
14. Koudelka T, Krejčí T, Kruis J (2018) Time integration of hypoplastic model for expansive clays. In: AIP conference proceedings, vol 1978. AIP Publishing
15. Machaček J, Staubach P, Tafili M, Zachert H, Wichtmann T (2021) Investigation of three sophisticated constitutive soil models: from numerical formulations to element tests and the analysis of vibratory pile driving tests. Comput Geotech 138:104276
16. Mašín D (2005) A hypoplastic constitutive model for clays. Int J Numer Anal Methods Geomech 29(4):311–336
17. Mašín D (2010) Predicting the dependency of a degree of saturation on void ratio and suction using effective stress principle for unsaturated soils. Int J Numer Anal Methods Geomech 34(1):73–90
18. Mašín D (2013) Clay hypoplasticity with explicitly defined asymptotic states. Acta Geotech 8:481–496
19. Mašín D (2014) Clay hypoplasticity model including stiffness anisotropy. Géotechnique 64(3):232–238
20. Mašín D (2017) Coupled thermohydromechanical double-structure model for expansive soils. J Eng Mech 143(9):04017067
21. Mašín D (2023) TRIAX user's manual. Charles University, Prague, Czech Republic. See https://soilmodels.com/triax
22. Mašín D, Khalili N (2008) A hypoplastic model for mechanical response of unsaturated soils. Int J Numer Anal Methods Geomech 32(15):1903–1926
23. Mašín D, Khalili N (2012) A thermo-mechanical model for variably saturated soils based on hypoplasticity. Int J Numer Anal Methods Geomech 36(12):1461–1485
24. Mašín D, Rott J (2014) Small strain stiffness anisotropy of natural sedimentary clays: review and a model. Acta Geotech 9:299–312
25. Matsuoka H, Nakai T (1974) Stress-deformation and strength characteristics of soil under three different principal stresses. In: Proceedings of the Japan society of civil engineers, vol 1974. Japan Society of Civil Engineers, pp 59–70
26. Ng CWW, Sun H, Lei G, Shi JW, Mašín D (2015) Ability of three different soil constitutive models to predict a tunnel's response to basement excavation. Can Geotech J 52(11):1685–1698
27. Ng CWW, Xu J (2012) Effects of current suction ratio and recent suction history on small-strain behaviour of an unsaturated soil. Can Geotech J 49(2):226–243
28. Ng CWW, Xu J, Yung S (2009) Effects of wetting-drying and stress ratio on anisotropic stiffness of an unsaturated soil at very small strains. Can Geotech J 46(9):1062–1076
29. Ng CWW, Yung S (2008) Determination of the anisotropic shear stiffness of an unsaturated decomposed soil. Géotechnique 58(1):23–35
30. Ng CWW, Zhou C (2014) Cyclic behaviour of an unsaturated silt at various suctions and temperatures. Géotechnique 64(9):709–720
31. Niemunis A, Herle I (1997) Hypoplastic model for cohesionless soils with elastic strain range. Mech Cohesive Frict Mater 2(4):279–299
32. Pedroso DM, Farias MM (2011) Extended Barcelona basic model for unsaturated soils under cyclic loadings. Comput Geotech 38(5):731–740
33. Poblete M, Fuentes W, Triantafyllidis T (2016) On the simulation of multidimensional cyclic loading with intergranular strain. Acta Geotech 11(6):1263–1285
34. Seidalinov G, Taiebat M (2013) Saniclay-b: a plasticity model for cyclic response of clays. In Proceedings of the sixty sixth Canadian geotechnical conference, pp 7
35. Sheng D (2011) Review of fundamental principles in modelling unsaturated soil behaviour. Comput Geotech 38(6):757–776
36. Stallebrass S, Taylor R (1997) The development and evaluation of a constitutive model for the prediction of ground movements in overconsolidated clay. Géotechnique 47(2):235–253
37. Svoboda J, Mašín D, Najser J, Vašíček R, Hanusová I, Hausmannová L (2023) BCV bentonite hydromechanical behaviour and modelling. Acta Geotech 18:3193–3211
38. Tafili M, Duque J, Ochmański M, Mašín D, Wichtmann T (2023) Numerical inspection of miner's rule and drained cyclic preloading effects on fine-grained soils. Comput Geotech 156:105310
39. Tafili M, Grandas C, Triantafyllidis T, Wichtmann T (2022) Constitutive anamnesis model (CAM) for fine-grained soils. Int J Numer Anal Methods Geomech 46(15):2817–2848

40. Tafili M, Medicus G, Bode M, Fellin W (2022) Comparison of two small-strain concepts: ISA and intergranular strain applied to Barodesy. Acta Geotech 17(10):4333–4358

41. Von Wolffersdorff P-A (1996) A hypoplastic relation for granular materials with a predefined limit state surface. Mech Cohesive Frict Mater Int J Exp Model Comput Mater Struct 1(3):251–271

42. Wang S, Wu W (2021) Validation of a simple hypoplastic constitutive model for overconsolidated clays. Acta Geotech 16:31–41

43. Wegener D, Herle I (2014) Prediction of permanent soil deformations due to cyclic shearing with a hypoplastic constitutive model. Geotechnik 37(2):113–122

44. Wichtmann T (2016) Soil behaviour under cyclic loading: experimental observations, constitutive description and applications. Habilitation. Karlsruhe Institute of Technology (KIT)

45. Wichtmann T, Fuentes W, Triantafyllidis T (2019) Inspection of three sophisticated constitutive models based on monotonic and cyclic tests on fine sand: hypoplasticity vs. sanisand vs. ISA. Soil Dyn Earthq Eng 124:172–183

46. Wichtmann T, Niemunis A, Triantafyllidis T (2007) Strain accumulation in sand due to cyclic loading: drained cyclic tests with triaxial extension. Soil Dyn Earthq Eng 27(1):42–48

47. Wichtmann T, Triantafyllidis T (2016) An experimental database for the development, calibration and verification of constitutive models for sand with focus to cyclic loading: part II-tests with strain cycles and combined loading. Acta Geotech 11:763–774

48. Wichtmann T, Triantafyllidis T (2016) An experimental database for the development, calibration and verification of constitutive models for sand with focus to cyclic loading: part I-tests with monotonic loading and stress cycles. Acta Geotech 11:739–761

49. Wichtmann T, Triantafyllidis T (2017) Strain accumulation due to packages of cycles with varying amplitude and/or average stress-on the bundling of cycles and the loss of the cyclic preloading memory. Soil Dyn Earthq Eng 101:250–263

50. Wichtmann T, Triantafyllidis T (2018) Monotonic and cyclic tests on kaolin: a database for the development, calibration and verification of constitutive models for cohesive soils with focus to cyclic loading. Acta Geotech 13:1103–1128

51. Wong KS, Mašín D (2014) Coupled hydro-mechanical model for partially saturated soils predicting small strain stiffness. Comput Geotech 61:355–369

52. Wong KS, Mašín D, Ng CWW (2014) Modelling of shear stiffness of unsaturated fine grained soils at very small strains. Comput Geotech 56:28–39

53. Xiong Y-L, Ye G-L, Xie Y, Ye B, Zhang S, Zhang F (2019) A unified constitutive model for unsaturated soil under monotonic and cyclic loading. Acta Geotech 14:313–328

54. Zhou C (2014) Experimental study and constitutive modelling of cyclic behaviour at small strains of unsaturated silt at various temperatures. PhD thesis